(Received 26 November 2023, Accepted 15 December 2023, Scheduled 19 December 2023)

Advances in Synthesis Strategies for Lanthanide-Based $NaYF_4$ Upconversion Nanocrystals and Their Applications in Ratiometric Thermometry

Raheel Ahmed Janjua[1,2], Wenbin Ji[2,3], Nayyar Abbas Shah[1], Julian Evans[1], Ruili Zhang[2], Sheng Zhang[4,5,*], and Sailing He[1,2,4,*]

[1] *Centre for Optical and Electromagnetic Research National Engineering Research Center for Optical Instruments, Zhejiang University, China*
[2] *Taizhou Hospital, Zhejiang University, Taizhou 318000, China*
[3] *Key Laboratory of Evidence-based Radiology of Taizhou, Linhai 317000, Zhejiang, China*
[4] *Ningbo Innovation Center, Zhejiang University, Ningbo 315100, China*
[5] *School of Mechanical Engineering, Zhejiang University, Hangzhou 310027, China*

ABSTRACT: The optical characteristics and varied applications of lanthanide-doped $NaYF_4$ upconversion nanocrystals have received considerable interest in recent years, such as in ratiometric thermometry. This review thoroughly examines the various synthesis processes utilized in producing these nanocrystals and their application in temperature sensing. Synthesis of $NaYF_4$ upconversion nanocrystals is a complex procedure that requires careful management of dopant concentrations, crystal phase, size, and shape. The distinctive luminescent characteristics of lanthanide ions, which facilitate the transformation of photons with low energy into emissions with higher energy, render $NaYF_4$ nanocrystals suitable for ratiometric thermometry applications. We explore the fundamental concepts underlying upconversion luminescence in developing ratiometric temperature sensors. In this discourse, we examine the selection of lanthanide dopants, the mechanics underlying their energy transmission, and the development of customized sensor architectures. This review covers the recent progress and utilization of $NaYF_4$ upconversion nanocrystals in ratiometric thermometry, including diverse areas such as biological temperature detection, environmental surveillance, and materials research. We evaluate the obstacles and potential advancements in this domain, specifically emphasizing approaches to improving temperature sensors' precision, responsiveness, and applicability based on upconversion.

1. INTRODUCTION

Up-conversion nanoparticles (UCNPs) have garnered significant interest in microscopy [1, 2], biomedical imaging [2–10], photodynamic therapy [11–17], and high-resolution imaging [18, 19] during the preceding decades due to their unique capability to absorb lower-energy photons and then emit higher-energy photons [20–24]. Up-converting nanoparticles (UCNPs) have several advantages, such as minimal background auto-fluorescence, limited cytotoxicity, and a substantial penetration depth for near-infrared (NIR) excitation light [25]. Recent advancements in plasmonics, metasurfaces, and metamaterials [26–33] could further enhance the emission efficiency of UCNPs. Furthermore, the incorporation of UCNPs with imaging methods such as Stimulated Emission Depletion (STED) microscopy offers an intriguing opportunity [17, 34]. STED microscopy utilizes the unique spectrum characteristics and photostability of UCNPs to potentially exceed the diffraction limit, allowing for more precise imaging of cellular structures [18, 35]. This integration aligns with the broader goal of advancing imaging capabilities by harnessing the unique properties of UCNPs [36–38]. The material composition of UCNPs significantly impacts their distinctive optical properties, including the host material, sensitized ions, and activated ions of lanthanide-based UCNPs [39, 40]. The main function of the matrix is to serve as a crystalline host lattice structure that facilitates the activation and sensitization of ions. The primary function of activated ions is to serve as luminous centers. Sensitized ions are responsible for absorbing near-infrared (NIR) light. The energy absorbed from the incident light can subsequently be transferred to the ions that have been activated, facilitating the emission of photons. Oxides, fluorides, and chlorides are frequently used to create UCNPs [41–44]. The selection of host materials based on metal fluorides has exhibited reliable chemical stability [45]. There have been numerous host matrix materials that have been documented. $NaYF_4$ is a highly effective host material for up-conversion luminescence (UCL) due to its low phonon energy ($< 400\,\mathrm{cm}^{-1}$) and high refractive index. These properties provide lower rates of nonradiative transitions and higher efficiency of energy transfer up-conversion (ETU) [46–48]. The compound $NaYF_4$ can manifest two crystallographic phases, specifically cubic and hexagonal. The hexagonal polymorph of $NaYF_4$ has a considerably higher upconversion efficiency than its cubic counterpart. Considerable research has been dedicated to fabricat-

* Corresponding authors: Sailing He (sailing@zju.edu.cn) and Sheng Zhang (szhang1984@zju.edu.cn).

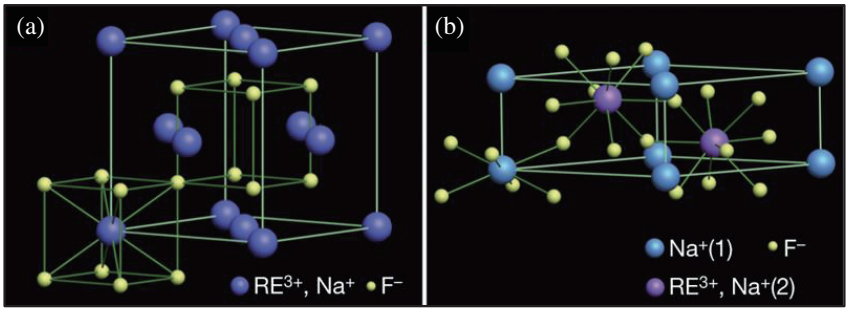

FIGURE 1. The phenomenon of phase transition in $NaREF_4$ structures induced by lanthanide doping is depicted schematically in (a) and (b). (a) represents the cubic-phase $NaREF_4$ structure, whereas (b) illustrates the hexagonal-phase $NaREF_4$ structure [106].

ing $NaYF_4$ materials with consistent dimensions and superior quality, encompassing various geometries [49–56]. The morphologies and sizes of $NaYF_4$ samples have a crucial role in determining their upconversion (UC) luminous features [57, 58]. Several investigations have been done to understand the effects of particle morphologies and sizes on radiative transition, nonradiative relaxation, energy transfer processes, and the UC luminescence of $NaYF_4$. There has been a notable increase in interest regarding the controlled synthesis, optical properties, and applications of nanoscale Ln^{3+}-doped $NaYF_4$. This keen interest can be attributed to the significant progress in nanotechnology, particularly in developing innovative methods for synthesizing materials. The $NaYF_4$ UCNPs exhibit distinctive optical characteristics and can potentially incorporate supplementary functional capabilities. Consequently, they can function as versatile probes with several modalities, catering to various applications that can be attributed to the unique architecture of the nanostructure [59–62]. Examining the temperature dependence of UC luminous behavior enhances the comprehension of the UC mechanism and the potential applications of these UC materials in temperature sensing and biosensors [63]. Temperature is a physical quantity important across various scientific disciplines. Its practical uses are particularly notable in precise measurement and calibration [64–66]. The field of temperature sensors has witnessed significant advancements in recent years, particularly in rare-earth doped ceramic phosphors and phosphor sensors [67–69]. Temperature sensing utilizing the response of optical materials is a highly appealing and complex area of research [70–74]. Contactless nano-thermometry with sub-microscale resolution has been widely utilized in several sectors, such as nanofluidic, catalytic processes, microelectronics, preclinical research, cell biology, and diagnostics [75–81]. Machine learning could be exploited to improve the performance of the temperature sensor, as it did successfully in many other sensing/imaging sectors (see e.g., [82, 83]). Optical thermometers can work in various challenging conditions, such as nanoscale, high voltage, and extreme conditions. Among several optical parameters, including emission intensity, spectrum shape, fluorescence lifetime, bandwidth, and spectral shift, Fluorescence Intensity Ratio (FIR) stands out as the most accurate and reliable optical parameter for temperature monitoring due to its remarkable ability to prevent self-referencing [84–87]. FIR-based upconversion nano-thermometry could also be applied in various fields, including anti-counterfeiting [88], optical rotation [89, 90], nonlinear properties [91, 92], temperature-controlled integrated circuit devices [93–95], temperature-sensitive cancer or antibiotic therapies [96, 97] and temperature calibration for gas sensing [98]. Nanoparticle ensembles have been prevalent in most temperature measurements based on upconversion nanoparticles [99–101]. Therefore, the spatial resolution of these measurements is determined by the diffraction limit of the stimulating laser beam. Measurements of individual nanoparticles provide spatial resolution determined by the size of the nanoparticle, which can be far smaller than the diffraction limit. Consequently, single-particle measurements offer a means to accomplish this level of precision [102–104].

The scope of this review includes the trajectory in synthesizing the most studied lanthanide-doped $NaYF_4$ particles, ranging from micro to nano and even sub-10 nanometer sizes, highlighting the advancements in fabrication techniques. Furthermore, it delves into the comprehensive scope of applications within nanothermometry, covering the recent strides made in leveraging unique properties of Ln-$NaYF_4$ for temperature-sensing applications at the nanoscale. This synthesis-to-application narrative encapsulates the evolving landscape of Ln-$NaYF_4$, encompassing both synthesis methodologies and thermometric developments.

2. LATTICE SYMMETRY

Under typical conditions, $NaYF_4$ can exist in two phases, i.e., cubic or hexagonal. The cubic phase undergoes a transition to a hexagonal phase at a temperature of 300°C, and the hexagonal form transforms into a high-temperature (HT) cubic phase beyond 400°C [105]. Rare earth elements can occupy different sites in two phases of $NaYF_4$. CaF_2 structures are formed in cubic phase $NaYF_4$ with one type of high-symmetry cation site, where Na+ and rare earth ions occupy the Ca^+ sites randomly,as shown in Figure 1(a). Ln-doped $NaYF_4$ crystal structure in the hexagonal phase comprises an ordered array of fluoride ions F^- that form a lattice. Na^+ sodium and Ln^{3+} lanthanide dopant ions occupy the cation positions of this lattice. The Na^+ and Ln^{3+} ions usually selectively occupy two types of low-symmetry cation sites in this hexagonal phase, as shown in Figure 1(b). The cations' surrounding electron clouds are dis-

torted to account for the crystal lattice's structural alterations. The arrangement and deformation of the crystal lattice are determined by the type and amount of lanthanide dopant added to the $NaYF_4$ host lattice [106].

3. SYNTHESIS TECHNIQUES

Several techniques have been developed for synthesizing Ln-$NaYF_4$ UCNPs with various sizes, morphologies, and architectures. The synthesis of $NaYF_4$ nanoparticles encompasses a variety of techniques to manipulate their dimensions, morphology, and characteristics accurately [107–110]. The synthesis of $NaYF_4$ represents a critical area of research in nanomaterial science owing to its unique optical and thermal properties. This compound, particularly when doped with rare earth ions, exhibits fascinating characteristics, making it invaluable for various applications such as bioimaging, photonics, and thermometry. Basic principles of nucleation, crystal formation, and surface chemistry are used to design nanocrystals with specific properties [111–113]. These techniques include thermal decomposition, co-precipitation, hydro(solvo)thermal, and microwave-aided approaches [114–116].

The synthesis of $NaYF_4$ nanomaterials involves the design and construction of nanoparticles since their distinct properties are utilized for specific purposes. Researchers strive to optimize the structure and composition of materials to use their capabilities in cutting-edge technologies. These technologies encompass various applications, such as high-resolution imaging and ultra-sensitive nanothermometry. The advancements in these fields have impacted multiple disciplines, including biomedical research, materials science, and optical engineering [117, 118].

4. SYNTHESIS OF MICROSCALE $NAYF_4$ PARTICLES

The most efficient UC material to date, Yb^{3+}- and Er^{3+}-doped $NaYF_4$, was first reported by Menyuk et al. in 1972 [119]. They treated a high-purity YF_3, YbF_3, and ErF_3 mixture in HF gas at 750°C, then dried and added a 20% excess desiccated NaF. Subsequently, the blend was heated at 200°C in purified argon for sixteen hours and further elevated to 1000°C for six hours to melt the sample. Since then, several studies have been devoted to synthesizing Ln-doped $NaYF_4$. In 2004, Kramer et al. revolutionized synthesis by presenting a novel and consistent approach for producing UC phosphor materials with high efficiency and excellent chemical and physical stability in the pure hexagonal phase. Additionally, they introduced a new structural model that considers the cationic distribution and inherent the nonstoichiometric nature of this phase. The optimization process included enhancing the phase purity, adjusting sodium content, fine-tuning the preparation temperature, optimizing doping levels, and controlling excitation power to maximize the green and blue phosphor's UC emission intensity [120]. In 2010, Zheng et al. employed an EDTA-assisted hydrothermal approach to synthesize β-$NaYF_4$ microcrystals co-doped with Yb^{3+} and Er^{3+}. Upon annealing, these microcrystals exhibited distinct emissions associated with Er^{3+} ions when excited at 980 nm. Notably, high-order UV UC emissions from Er^{3+} were detected, and these UV emissions were contingent on the pump power density of the 980 nm NIR light, potentially involving four- or five-photon UC processes [121]. Som et al. recently synthesized Microparticles of hexagonal $NaYF_4$ co-doped with Er^{3+} and Yb^{3+} using a microwave-enhanced hydrothermal method, resulting in uniform morphology and a pure phase within a shorter reaction time, which is shown in Figure 2. The reaction parameters influenced the phase and morphology, with a notable transformation from cubic to hexagonal phase as the reaction duration increased from 10 minutes to 2 hours at 180°C. Optimized conditions yielded β-$NaYF_4$ micro prisms with narrow size distributions and enhanced UC emission peaks at 524 nm, 545 nm, and 659 nm upon 980 nm excitation, attributed to Er^{3+} ion transitions [122].

5. SYNTHESIS OF NANOSCALE $NAYF_4$ PARTICLES

Many studies concentrate on creating and analyzing superior lanthanide-doped cubic and hexagonal $NaYF_4$ particles. The tendency of the particles to arrange themselves into uniform nanoplates or rods within the micrometer and sub-micrometer size range presented challenges in developing a practical method for producing small hexagonal nanoparticles.

Zeng et al. synthesized hexagonal-phase Yb^{3+}, Er^{3+}-doped $NaYF_4$ nanoparticles in 2004 for the first time with an average dimension of 25 nm in a solution of acetic acid [56]. Zhang et al's technique, originally proposed to fabricate the uniform LaF_3 particles was employed to synthesize $NaYF_4$ and yielded significant improvement in the size, shape, and uniformity of the UCNPs [123]. Several research groups have significantly improved this process, resulting in its widespread use as a standard method for producing monodisperse and orderly $NaYF_4$ nanocrystals in cubic and hexagonal configurations. The technique relies on the thermal decomposition of trifluoroacetate within a solvent mixture of oleic acid and octadecene [124–131].

Yi et al. demonstrated the co-precipitation of RE chlorides with NaF in the environment of ethylenediamine tetraacetic acid (EDTA) to achieve the cubic phase of Yb^{3+} and Er^{3+} doped $NaYF_4$ particles. This approach yielded spherical particles with a diameter ranging from 32 to 46 nm with a limited size distribution. These particles transformed into larger particles with the hexagonal phase when their dry powders were annealed between 400°C and 600°C. The resulting hexagonal particles also showed significant UC luminescence efficiency [111].

Yi and Chow extended the synthesis process to produce $NaYF_4$ with reduced dimensions. They observed that when the breakdown was carried out in pure oleylamine at 330°C, very small hexagonal $NaYF_4$:Yb^{3+}, Er^{3+} nanoparticles were produced. This is the first time that β-$NaYF_4$ particles, measuring 10 nm in size, have been effectively synthesized. These particles had a restricted size distribution and consistent morphologies. Consequently, they could be distributed and easily suspended in organic solvent. The particles exhibited a uniform shape and a limited size range, as determined by dynamic light

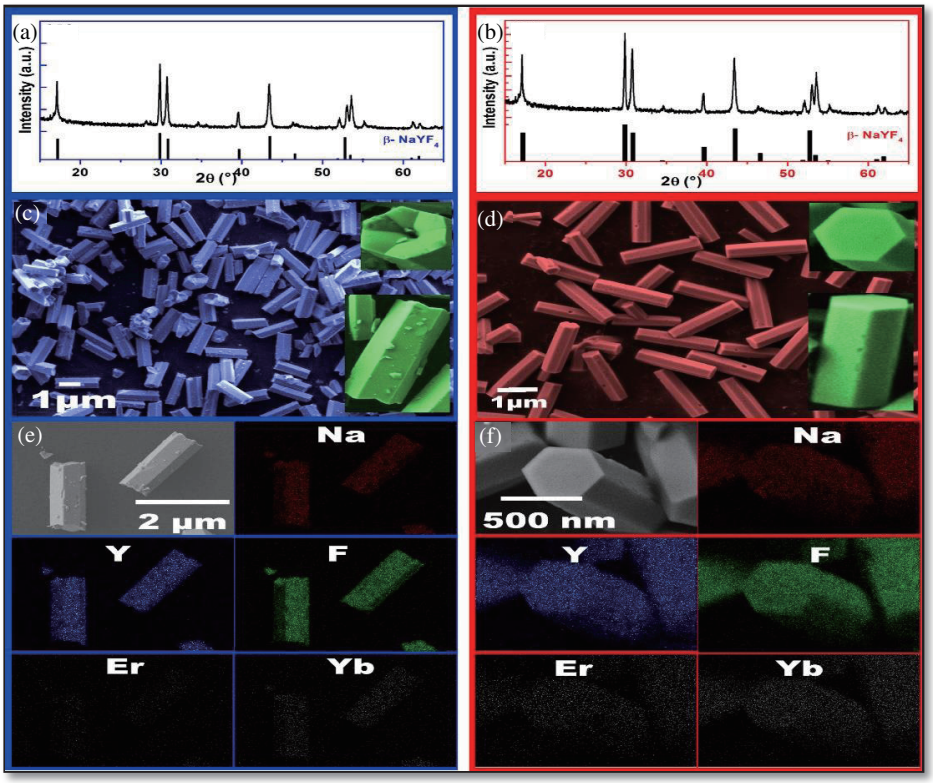

FIGURE 2. X-ray diffraction patterns, field emission scanning electron microscopy, and the respective elemental mapping were performed on $NaYF_4$ microcrystals doped with 2 mol% Er^{3+} and 18 mol% Yb^{3+}. These microcrystals were synthesized using two different methods: ((a), (c) & (e)) hydrothermal method (HM) and ((b), (d) & (f)) microwave hydrothermal method (MWHM) [122].

scattering (DLS) and transmission electron microscopy (TEM) measurements, indicating a size of 11 nm [129].

Boyer et al. produced $NaYF_4$ nanoparticles doped with lanthanides in the cubic phase. The nanoparticles displayed an average size of 27.6 nm with a standard deviation of 1.6 nm [128]. Using trifluoroacetate throughout the synthesis process produces reactive fluoride compounds quickly at high temperatures. However, reproducibility problems arise due to several drawbacks, such as generating hazardous gases, elevated reaction temperatures, and a relatively narrow temperature range (less than 10°C) for decomposition [132]. As a result, efforts were undertaken to create substitute synthesis techniques that provide the nanoparticles with the desired phase, geometry, and dimensions.

Li and Zhang developed various techniques to produce $NaYF_4$ nanocrystals with a pure hexagonal phase. Their method combines oleic acid and octadecene solvents at 300°C [133]. They used *in-situ* produced rare-earth oleates, NaOH, and NH_4F instead of metal trifluoroacetate. As an alternative, oleic acid was substituted with stearic acid and trioctylphosphine oxide (TOPO), and octadecene was swapped out for a mixture of eicosene and trioctylamine as a high-boiling solvent. The final particles showed remarkable quality in shape homogeneity, forming hexagonal plates and nanospheres based on oleic acid content, with a size distribution centered around 21 nm [134].

Liu et al. developed a technique that successfully created doped β-$NaYF_4$ nanoparticles with exceptional consistency in size and an extremely narrow range of sizes, measuring (28.25 ± 0.76) nm. They employed a synthetic approach with NaF and RE oleates as precursors. Nanotubes consisting of closely packed, uniform nanocrystals were produced by impregnating α-$NaYF_4$ nanocrystals doped with Er^{3+} and Yb^{3+} into a spongy, anodized aluminum oxide (AAO) membrane. Emission bands were seen in the green, red, and blue spectrum regions, respectively, when Yb^{3+}, Er^{3+}, and Yb^{3+}, Tm^{3+} ions were doped into cubic or hexagonal $NaYF_4$ nanocrystals [132].

Several studies explored methods to increase the spectrum of colors that emit light. Ehlert et al. demonstrated the broadening of emission color's range by combining colloids of upconversion nanoparticles with varying dopant ions. They synthesized and mixed UCNPs in varying proportions to form colloids. The colloids consisting of Ln-doped $NaYbF_4$ exhibit emission bands in green and red regions of the spectrum. In particular, $NaYbF_4$:Er^{3+} and $NaYbF_4$:Ho^{3+} exhibit mostly blue and infrared (IR) emissions, whereas $NaYbF_4$:Yb^{3+} and $NaYbF_4$:Tm^{3+} emit both in blue and IR Regions [135]. Wang and Liu doped the $NaYF_4$ host with three ions (Yb^{3+}, Tm^{3+}, Er^{3+}) simultaneously and controlled their concentration to achieve a variety of overall color outputs. They witnessed the shift from bluish to whitish for $NaYF_4$:Yb^{3+}, Tm^{3+}, Er^{3+}, whereas greenish-yellowish to reddish for $NaYF_4$:Yb^{3+}, Er^{3+} by controlling the concentration of dopants [136].

The oleate-based synthesis approach has several advantages, including a narrower particle size distribution, higher luminescence efficiency, and a higher level of phase purity in the final UCNPs. The synthesis of the α-phase is produced at lower temperatures below 300°C, demonstrating that the process in oleic acid is kinetically regulated despite the thermodynamic preference for the hexagonal bulk phase at low temperatures [137, 138].

6. SYNTHESIS OF SUB-10 NANOMETER NAYF$_4$ PARTICLES

Nanocrystals with outstanding optical characteristics have demonstrated potential as tools for biological imaging [3]. An essential criterion for bioimaging applications is the biocompatibility of the nanocrystals. In many experiments, it is necessary for the nanocrystals to have a similar size to (or smaller than) the biomolecules they are labeling in order to avoid any disruption to cellular systems [139]. UCNPs show great potential as probes for single-particle tracking. Thus, the synthesis of sub-10-nm $NaYF_4$, which is the crystal structure that exhibits the most efficient UC, is in high demand. Furthermore, there are uncertainties regarding whether small $NaYF_4$ nanocrystals would maintain the exceptional optical properties observed in larger UCNPs [140].

A group of researchers successfully produced sub-10 nm luminescent $NaYF_4$ nanocrystals that created clear colloidal solutions. Where N-(2-hydroxyethyl)ethylenediamine (HEEDA), in a high-boiling solvent, was treated to co-precipitate $NaYF_4$:Yb^{3+}, Er^{3+}, and $NaYF_4$:Yb^{3+}, Tm^{3+} nanoparticles [141]. Transparent colloidal solutions of cubic-phase particles were obtained using this method. The upconversion efficiency of these solutions has been reported to be about eight orders of magnitude higher than the lanthanide-doped phosphate nanocrystal colloids [142]. Nevertheless, despite significantly improving earlier techniques, this synthesis procedure has several shortcomings, including a relatively broad particle size dispersion ranging from 5 to 30 nm and the generation of the less effective α-phase of $NaYF_4$ [111, 133, 136, 142].

Schäfer et al. have shown that even at room temperature, nanocrystalline β-phase $NaYF_4$ may be produced through a straightforward solid-state reaction combining NH_4F, Na_2CO_3, and RE carbonates [143]. Hexagonal-phase $NaYF_4$ nanocrystals are produced when this reaction occurs in oleylamine or a combination of oleylamine and oleic acid. Their particle size distribution is usually wider, spanning from 4 to 10 nm. Additionally, incorporating Gd^{3+} ions has shown to be an effective means of improving phase and size control. Wang and his colleagues performed the synthesis of $NaYF_4$:Yb^{3+}, Er^{3+} nanocrystals at various doping concentrations and introduced Gd^{3+} ions into the nanocrystals to synthesize a ternary doped system. Under the selected reaction conditions, a blend of cubic and hexagonal phases has been observed without additional Gd^{3+} ions. However, the shift in structure from cubic to hexagonal was more noticeable, and the matching particle sizes shrank as Gd^{3+} concentrations rose. The visible color of the upconverting nanocrystals was adjusted by using Gd^{3+} with binary-doped $NaYF_4$:Yb^{3+}, Er^{3+}, or ternary-doped $NaYF_4$:Yb^{3+}, Er^{3+}, Tm^{3+}, which produced the ternary and quaternary doped lanthanide species.

Wang et al. achieved particle size reduction to below 10 nm by introducing gadolinium as a partial substitute for yttrium. They analyze a material system where doping influences the growth process, enabling precise manipulation of the resultant nanocrystals' crystallographic phase, size, and optical emission properties. They demonstrate that by precisely incorporating trivalent Ln-dopant ions at controlled concentrations, it is possible to systematically customize the dimension (down to 10 nm), phase (cubic or hexagonal)along with upconversion emission color of $NaYF_4$ nanocrystals [106]. Ostrowski et al. [140] fabricated approximately uniform sub-10 nm UCNPs. They outline the parameters for precise fabrication of protein-sized β-phase $NaYF_4$ nanocrystals doped with 20% Yb^{3+} and 2% Er^{3+}, ranging in diameter from 4.5 to 15 nm. The nanocrystal size was controlled by adjusting the proportion of primary surfactants, the Y^{3+}:F^- ratio, and the temperature range for the reaction, influencing their crystalline phase. Longer reaction durations promoted the generation of the intended β-phase nanocrystals with a relatively minor impact on nanocrystal dimensions [144]. Rinkel et al. also prepared sub-10 nm particles but employed decantation or other methods to eliminate residual NaF due to excessive fluoride source usage. The synthesis of 5 nm β-$NaYF_4$:Yb, Er core particles involves the reaction between sodium oleate, RE oleate, and ammonium fluoride. This reaction uses the favorable sodium to RE ion ratio, which facilitates the construction of a significant amount of β-phase seeds, resulting in the desired core particles. Subsequently, a sodium yttrium fluoride ($NaYF_4$) shell with a diameter of 2 nm is produced by employing 3–4 nm α-$NaYF_4$ particles as a precursor for the β-phase shell material shown in Figure 3. Contrary to the core particles, the α-phase particles are created using an intentionally low sodium-to-RE ion ratio. This low ratio effectively inhibits the formation of undesirable β-$NaYF_4$ particles during the expansion of the shell [145, 146].

The first author's research group synthesized the nanocrystals in a complex blend comprising Oleic acid (OA) and Octadecene (ODE) at a 3 : 1 ratio. A higher quantity of OA was utilized as it demonstrated superior capabilities for dissolving RE elements and sodium compared to ODE [105]. When a more significant proportion of ODE is employed, particle aggregation occurs at the OA and ODE interface due to the restricted solubility of precursors in ODE, resulting in larger particles. Conversely, a greater concentration of OA reduces the chances of monomers adhering to the nucleated crystal. The presence of a minimal amount of ODE prevents nanocrystal agglomeration.

The evolution of synthesizing $NaYF_4$ particles has traversed various scales, from micro to nanoscale, each realm offering unique challenges and advancements. In the macroscopic domain, Menyuk et al. laid the groundwork in 1972 [119], employing a rigorous process to yield Yb^{3+}- and Er^{3+}-doped $NaYF_4$, a significant milestone. Subsequently, studies like Kramer et al. in 2004 [120] refined the synthesis, prioritizing efficiency, stability, and phase optimization, setting a benchmark for subsequent techniques. The quest for microscale par-

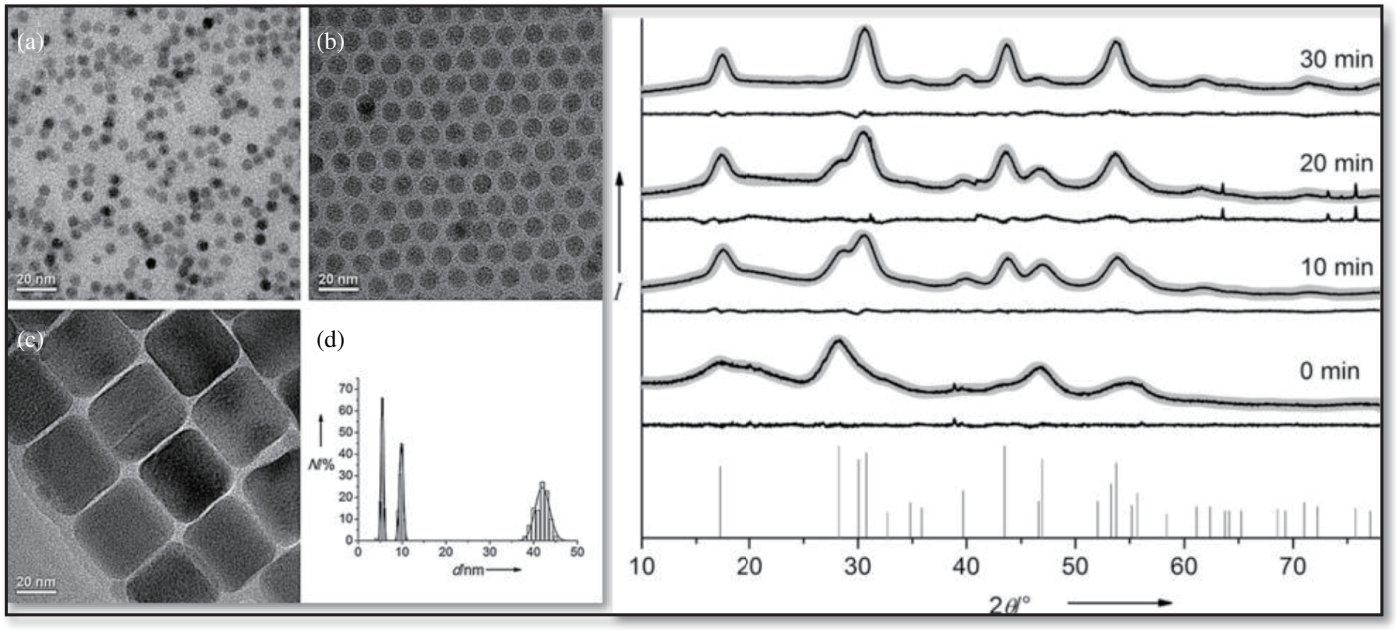

FIGURE 3. (a), (b) & (c) shows transmission electron microscopy (TEM) pictures obtained for nanoparticles provided with (d) histogram. The data sets are subjected to Rietveld refinements, as the solid lines indicate. The initial outcome consists of minute particles of α-phase $NaYF_4$:Yb,Er [145].

ticles witnessed innovative approaches by Zheng et al. [121] and Som et al. [122], leveraging hydrothermal and microwave-enhanced methods, respectively, to achieve controlled morphologies and distinct emission behaviors, unlocking the potential for higher-order UV emissions in Er^{3+}-doped microcrystals.

At the nanoscale, the landscape is rich with diverse synthesis methodologies. The pioneering work of Li et al. and Yi et al. marked the synthesis of small hexagonal-phase $NaYF_4$ nanoparticles, catalyzing subsequent advancements in controlling size, shape, and dispersion. The oleate-based synthesis method emerged as a frontrunner, offering superior luminescence and phase purity, although challenges persisted regarding narrow temperature ranges and hazardous gas production. Efforts to craft sub-10 nanometer particles ensued, with researchers using meticulous control over parameters such as surfactant concentration, reaction duration, and fluoride sources. Wang et al. and Ostrowski et al. demonstrated the pivotal role of doping in achieving precise control over crystallographic phase, size, and optical properties, enabling tailored nanocrystals even below ten nanometers. Rinkel et al. faced hurdles with excessive fluoride sources, necessitating extra purification steps. Each synthesis scale presents its own set of limitations and triumphs. Whether navigating microscale precision or delving into the nanoscale realm for tailored crystals, researchers have tirelessly pursued advancements, harnessing intricate methodologies to shape the future of $NaYF_4$ particle synthesis.

7. PROS AND CONS OF $NAYF_4$ SYNTHESIS METHODS

The synthesis of $NaYF_4$ nanoparticles has evolved from macro to micro and sub-10 nanometer scales. Methods like thermal decomposition and co-precipitation set the stage for newer techniques like hydro(solvo)thermal and microwave approaches. Scientists choose particular methods, aiming to customize nanoparticles for uses in bioimaging, photonics, and temperature measurement.

Thermal Decomposition: Menyuk et al. [119] pioneered the synthesis of Yb^{3+} and Er^{3+} doped $NaYF_4$ using a rigorous process involving high temperatures. This method efficiently produces nanoparticles with controlled properties, but it suffers from challenges such as reproducibility issues due to the high-temperature requirements and the generation of hazardous gases.

Co-precipitation: Kramer et al. [120] refined the co-precipitation method, emphasizing efficiency, stability, and phase optimization. While simpler compared to other methods, co-precipitation might yield mixed phases and require additional steps to achieve precise nanoscale properties.

Hydro(solvo)thermal: Wang et al. [147] and Zheng et al. [121] employed a hydrothermal method to create nanoparticles with specific shapes and unique light emission properties. However, this process might struggle to scale up for larger production because it takes more time to react and can be quite sensitive to the exact conditions under which the reaction occurs.

Co-precipitation with EDTA: Yi et al. [129] demonstrated co-precipitation with EDTA to achieve cubic-phase Yb^{3+}, and Er^{3+} doped $NaYF_4$ particles with limited size distribution. While offering controlled properties and efficient luminescence, this method might encounter challenges in controlling phase transitions and scalability.

Microwave-aided approaches: Som et al. [122] used a microwave-enhanced hydrothermal method to synthesize hexagonal-phase $NaYF_4$ micro prisms with enhanced UC emission peaks. This method reduces the reaction time and

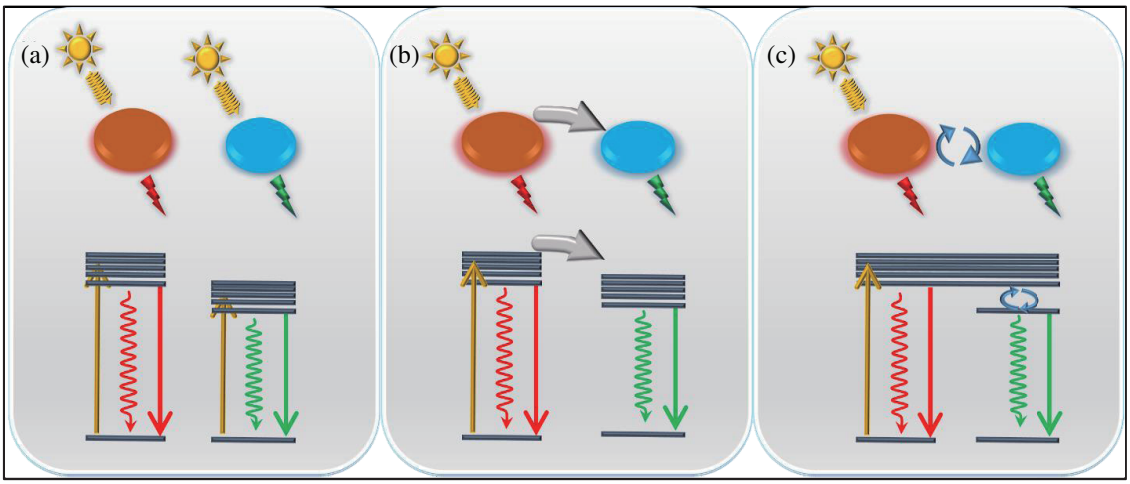

FIGURE 4. Schematic summaries of three different electronic structures leading to dual emission. Illustrations depicting (a) two UCL centers that are thermally independent, (b) moderately dependent, and (c) thermally coupled.

offers uniform morphology, but optimizing parameters and achieving precise control over size is not easy.

Each method showcased specific advantages and limitations. These examples illustrate how researchers have navigated various synthesis techniques, each offering distinct advantages and limitations, to engineer $NaYF_4$ nanoparticles tailored for specific applications in bioimaging, photonics, and thermometry.

8. BACKGROUND OF THE FLUORESCENCE INTENSITY RATIO

The optical temperature measurement technique utilizing the FIR has attracted significant attention owing to its exceptional precision and sensitivity. Its reliance on intensity ratios makes it immune to unwanted factors, rendering this luminescence-based thermometry method more effective. Its self-referencing nature eliminates the necessity for a temperature benchmark. It can be implemented using emission lines from various combinations of lanthanides and transition metal ions, each with distinct temperature responses, either from a single source or multiple luminescent centers. In recent years, this method has been extensively documented as a primary luminescence-based thermometric approach [148]. Studies outlined three scenarios related to the coupling modes of two excited states, spanning from "thermally non-coupled" to "moderately coupled" and "strongly coupled," shaping the foundation for constructing FIR through dual emission. However, achieving dual emissions presents a challenge in managing the temperature dependency difference between the two emissions [149].

Numerous techniques have been explored to create dual emission systems with differing temperature dependencies, classified into three groups based on how energy transfer affects the temperature dependence between excited states shown in Figure 4. Approach1 indicates scenarios where the temperature has no impact on energy transfer, suitable for "non-coupled" emission scenarios. Conversely, Approach II demonstrates temperature-sensitive energy transfer between electronically "moderately coupled" states. Approach III, relevant to strongly linked states like thermally coupled luminescent (TCL) pairs, relies on temperature-driven population distribution via the Boltzmann distribution [150].

TCL pairs, particularly involving lanthanide ions due to their multiple intermediate energy levels, have been a focus for FIR-based thermometric applications. The potential lies in the vast energy level pairs satisfying the essential level separation criterion for TCL. Although more significant level separations benefit relative sensitivity, the stringent energy spacing $\Delta E < 2000\ cm^{-1}$ criterion remains a limiting factor, crucial for strong coupling and relative sensitivity determination. However, fluorescence peak overlaps due to small spacing may affect signal discernibility and deviate from predicted FIR behavior.

Considering the challenges of tightly coupled excited states, alternative approaches using Ln^{3+} doped $NaYF_4$ offer promising avenues. Ln^{3+} ions in inert materials have intra-4f transitions, which are inert to temperature fluctuations, allowing for feasible thermometric designs-based and non-coupled levels by leveraging thermal quenching among various activators. Additionally, the prolonged lifetime of most Ln^{3+} excited states facilitates energy transfer between "moderately coupled" levels, enabling temperature-sensitive efficiency.

In the following section, we explore recent advancements in compensating for shortcomings observed in FIR routes. It delves into methods utilizing Ln^{3+} luminescence for FIR-based temperature sensors. It highlights novel approaches that overcome the limitations of excited states, focusing on strategies I, II, and III FIR thermometry based on Ln^{3+} doped $NaYF_4$ luminescence.

9. ASSESSMENT OF THERMOMETER EFFECTIVENESS

Assessing the performance of a thermometer involves quantifying its effectiveness based on absolute and relative thermal sensitivities, temperature resolution, and repeatability. Here, we'll initially outline and summarize the meanings of these key indicators.

10. THERMAL SENSITIVITIES

The absolute thermal sensitivity (Sa) represents the rate of alteration in thermometric characteristics (denoted by D) during a temperature transition (qT) [72].

$$S_a = \frac{qD}{qT}$$

Comparing the performance of thermometers using absolute sensitivity becomes challenging when different materials or physical principles are employed. To address this, relative thermal sensitivity (Sr) emerges, aiming to alleviate this issue of comparison between thermometers with diverse natures. It is typically represented as a percentage change per degree of temperature alteration ($\%\,K^{-1}$) [68].

$$S_r = \frac{1}{D}\left|\frac{qD}{qT}\right|$$

The relative thermal sensitivity (Sr) plays a critical role in determining the temperature readout accuracy of a luminescent thermometer.

11. TEMPERATURE RESOLUTION

A thermometer's minimum detectable temperature change is termed temperature resolution or temperature uncertainty (denoted by dT), typically measured in Kelvin. This parameter relies on the specifics of the measurement apparatus, including the experimental detection configuration and the signal-to-noise ratio [63].

$$dT = \frac{1}{Sr}\frac{qD}{D}$$

12. REPRODUCIBILITY AND REPEATABILITY

Reproducibility refers to the fluctuations observed in the precise measurement carried out under distinct conditions, such as using different methods or devices. Repeatability measures a thermometer's capability to produce consistent results under varying conditions [148].

13. FIR BETWEEN THERMALLY COUPLED LEVELS

Strong coupling can be produced between two energy levels whose energy gaps fall between 200 and 2000 cm^{-1}. The Boltzmann distribution is obeyed by the relative population between these two levels [151]. This distribution offers the capability to monitor temperature using a ratiometric approach. Consequently, the FIR equation can be recast as follows:

$$\mathrm{FIR} = \frac{I_2}{I_1} = \frac{g_2 A_2 h\vartheta_2}{g_1 A_1 h\vartheta_1} = C\exp\left(-\frac{\Delta E_{21}}{k_B T}\right)$$

where Ix, gx, Ax, and ϑx denote the emission intensity, degeneracy, spontaneous emission rate, and frequency of the thermally linked energy levels ($x = 1, 2$), respectively, and C, h, and Kb denote the constants of proportionality, Planck, and Boltzmann, respectively. Here ΔE_{21} and T stand for the difference in energy levels and absolute temperature in order.

Vetron et al. [101] pioneered the utilization of fluorescence intensity to showcase the potential of the temperature-sensitive green emission from fluorescent $NaYF_4$:Er^{3+}, Yb^{3+} nanoparticles. This approach demonstrated the viability of these nanoparticles as thermal nanoprobes for sensing temperatures within liquids and HeLa cervical cancer cells. Later, heavily Nd^{3+} doped $NaYF_4$ nanoparticles were employed for temperature assessment. Temperature evaluation was achieved by measuring the intensity ratio between the two Stark components within the $^4F_{3/2}$ multiplet in the Nd^{3+} ions [152]. In another work, the utility of $NaYF_4$:Er^{3+}, Yb^{3+} nanocrystals (NCs) and $NaYF_4$:Er^{3+}, Yb^{3+}/SiO_2 core/shell ($NaYF_4$@SiO_2) NCs as UC nanothermometers has been explored. These uniform core UCNPs exhibited thermally governed UC luminescence up to 600 K, but their luminescence diminished at elevated temperatures owing to ligand oxidation and NC agglomeration. They further developed a silica coating around the core NCs to address this by generatingcore/shell NCs. The $NaYF_4$@SiO_2 NCs demonstrated consistent thermally induced UC luminescence up to 900 K, showcasing remarkable resilience during repeated cycling between 300 and 900 K [153]. The measurements exhibited a high level of precision, with standard fluctuations ranging from 1 to 5 K below and above 750 K. This study highlights temperature-sensitive probes, Yb^{3+} and Er^{3+} doped $NaYF_4$ encapsulated in a safeguarding silica shell, ranging up to 900 K. This fluorescence-based infrared thermometry extended temperature range, durability, and noninvasive nature which makes it suitable for diverse systems and remote temperature sensing applications. In a study conducted by Li and coworkers [154], the antiwhite LED (light emitting diode) capabilities of luminescence ratiometric thermometry were explored using Er^{3+} as a proof-of-concept. The investigation centered around the upconversion (UC) energy transition from $^2H_{11/2}$/$^4S_{3/2}$ to $^4I_{15/2}$ & $^4G_{11/2}$/$^2H_{9/2}$ to $^4I_{15/2}$ states of Er^{3+} embedded in $NaYF_4$. The longer emission lines of 520 and 540 nm overlapped entirely with the white LED emission spectrum, whereas the shorter peaks at 390 and 410 nm showed no significant spectral overlap with the white LED spectrum. This distinction allowed for comparing these two emission lines within the same material. The scheme is shown in Figure 5(a). Their findings showed that the $^4G_{11/2}$/$^2H_{9/2}$-$^4I_{15/2}$ transitions remained unaffected by the white LED irradiation. Conversely, the transition from $^2H_{11/2}$/$^4S_{3/2}$ to $^4I_{15/2}$ displayed a noticeable dependence on the white LED lighting under similar conditions. The study concluded that, in scenarios where white LED irradiation cannot be disregarded, the 380/409 nm emission bands offer a significantly better choice than the 520/540 nm bands for precise thermometric measurements. The emission band ratios of water-dispersible core@shell exhibit a temperature dependence that is non-overlapping and specific to Yb^{3+}/Er^{3+}. The study focused on examining $NaYF_4$:Yb^{3+}:Er^{3+}@SiO_2 nanorods throughout the I-BW (biological window) and II-BW spectral regions, as illustrated in Figure 5(b) [155]. Specifically, the $^2F_{5/2}$ $\rightarrow$$^2F_{7/2}$/$^4F^{9/2}$ $\rightarrow$$^4I_{15/2}$ corresponding

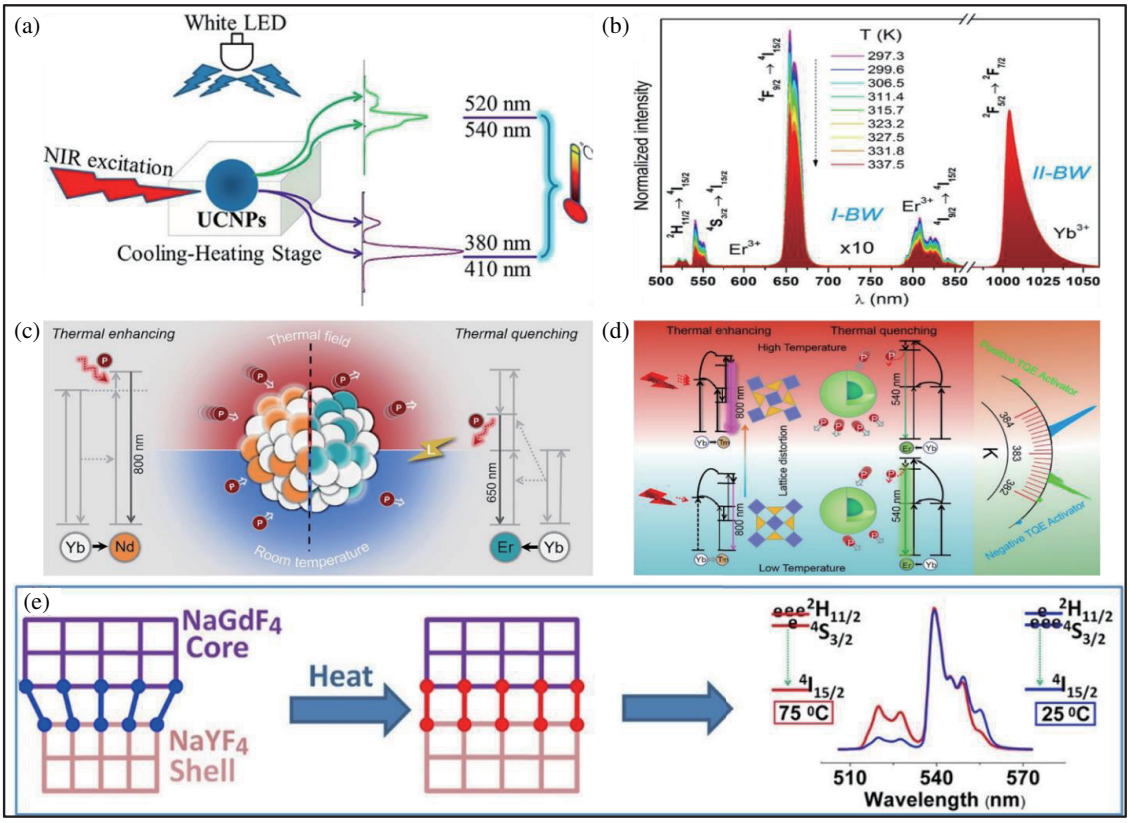

FIGURE 5. (a) illustrates the experimental arrangement for measuring temperature using $NaYF_4$:40%Yb^{3+}, 2%Er^{3+} upconversion nanoparticles (UCNPs). (b) emission spectra of $NaYF_4$:Yb^{3+}−Er^{3+}@SiO_2 NRs; $\lambda ex = 975$ nm. (c) illustrating the process of interface lattice self-adaptation. (d) demonstrates a temperature sensitivity by combining the positive and negative thermal quenching phenomena. (e) Proposal for developing ultrasensitive ratiometric nanothermometers with excellent contrast [154–158].

to 1010/810 nm and $^2F_{5/2} \rightarrow ^2F_{7/2}/^4F_{9/2} \rightarrow ^4I_{15/2}$ corresponding to 1010/660 nm transitions were exploited for temperature-sensing purposes. These exhibited dual-center emissions, effectively combining bright UC luminescence from Er^{3+} and a conventional down-shifting emission from Yb^{3+}. The study highlighted the advantages of employing near-infrared (NIR) Yb^{3+}/Er^{3+} band ratios for temperature sensing over the Er^{3+} 525/545 nm band ratio, primarily due to the superior light penetration capabilities through tissues. This preference was validated through a straightforward *ex vivo* experiment, affirming the effectiveness of the selected NIR band ratios for practical applications in temperature sensing. Another development in temperature-responsive nanoparticles showcased a remarkable sensitivity of 9.6% K^{-1} at room temperature and extending beyond 2.3% K^{-1} up to 413 K, which is suitable for ratiometric thermometry. Their approach comprises heterogeneous nanostructures, offering finely tuned thermal responses achieved through controlled nanoparticle growth. The scheme of their approach is shown in Figure 5(c). This design provides exceptional sensitivity and stability in these ultrasensitive nanothermometers, enabling prolonged noncontact monitoring of localized heat dissipation in microelectronic devices. In addition, the implementation of thermally enhanced anti-Stokes emission using ytterbium and neodymium lanthanide ions led to a remarkable improvement of more than ten times in both sensitivity and dynamic range when compared to traditional ytterbium and erbium-codoped nanothermometers [156]. An innovative approach to create ultrahigh-sensitive temperature probes involves incorporating both positive and negative thermal quenching phenomena within a hydrogel matrix [157]. The methodology exploits the positive thermal quenching effect observed in Er^{3+} ions within Yb/Er:$NaYF_4$@$NaYF_4$ nanocrystals, contrasted with the negative thermal quenching effects seen in Nd^{3+} and Tm^{3+} ions within a $Yb_2W_3O_{12}$ material in bulk form as shown in Figure 5(d). Over the temperature span from 313 to 553 K, the fluorescence intensity ratios of Er to Nd and Tm to Er exhibited striking changes, decreasing by about 1654 times and increasing by 14,422 times, respectively. This achieved maximum relative sensitivities of 15.3% K^{-1} at 553 K and 23.84% K^{-1} at 380 K. The approach suggested by this study demonstrates a promising avenue for highly sensitive probes utilizing lanthanide ion-doped materials. Subsequently, Wu et al. [158] introduced another method that leverages lattice self-adaptation to enhance the thermal sensitivity of UCNPs significantly. Their study used the temperature-sensitive FIR of the dopant Er^{3+} as an indicator of temperature fluctuations. They engineered a heterojunction of $NaGdF_4$/$NaYF_4$ as the host material, deliberately inducing lattice distortion at the interface that responded sensitively to temperature changes as

shown in Figure 5(e). As the temperature increased, the FIR associated with the transitions $^2H_{11/2}/^4S_{3/2} \rightarrow ^4I_{15/2}$ demonstrated a surge. This was accompanied by a self-adaptive reduction in interface lattice distortion, contributing to an additional increase in the FIR. By employing core/shell upconversion nanoparticles capable of lattice self-adaptation, they achieved a substantially heightened thermal sensitivity three times greater than that observed in core-only nanoparticles. A set of fluoride nanocrystals was synthesized, $NaYF_4$:$Nd^{3+}$and $NaGdF_4$:Nd^{3+}, with Nd^{3+} ion concentrations ranging from 0.1% to 50% and sizes under 20 nm through thermal decomposition. The effects of dopant ion concentration and material characteristics on spectroscopic and thermometric properties across a broad temperature spectrum from 200 to 473 K were examined [159]. The study used two excitation wavelengths, 793 nm and 1060 nm, corresponding to the absorption from the ground and excited states, respectively. The purpose was to evaluate the appropriateness of the materials for single-band ratiometric luminescence thermometry. The 793 nm wavelength was chosen due to its high absorption cross-section in the near-infrared range, which is crucial for potential biological applications. Temperature determination relied on the emission intensity at 880 nm associated with the $^4F_{3/2}/^4I_{9/2}$ electronic transition under the mentioned excitation conditions. Increasing the Nd^{3+} concentration from 0.1% to 50% expanded the usable temperature range from 200 K to 250 K in the $NaYF_4$ host and 235 K to 270 K in the $NaGdF_4$ nanocrystals. The most significant relative sensitivities were observed in materials doped with 50% Nd^{3+} ions, irrespective of the host. These achieved 16.9% K^{-1} at 223 K for $NaYF_4$:50%Nd^{3+} and 16.3% K^{-1} at 203 K for $NaGdF_4$:50%Nd^{3+}. Although the sensitivity reduced with increasing temperature, it consistently remained above the critical 1% K^{-1} threshold across the analyzed temperature range. These exceptionally high values signify the substantial potential of the investigated nanocrystals for luminescence-based thermometry applications.

14. FIR BETWEEN MODERATELY COUPLED LEVELS

The inherent robustness of 4f electrons compared to the outer $^5S_2$ and $^5P_6$ shells results in their relative insensitivity to temperature changes. When inert materials are doped with Ln^{3+} ions, this characteristic allows for the feasibility of thermometric designs employing a range of thermal quenching techniques across various activator categories. Additionally, the extended lifetime of individuals can be attributed to the excited states of Ln^{3+} ions due to the 4f-4f dipole transitions which are parity forbidden. These transitions facilitate the efficient exchange of excitation energy between diverse excited states, creating ample room for developing temperature-sensitive thermometric designs utilizing energy transfer efficiency among "moderately coupled" levels.

$NaYF_4$:Yb^{3+}, Er^{3+}, Nd^{3+} and $NaAlSiO_4$:Cr^{3+} dual-phase glass ceramics were effectively constructed using a melt-quenching procedure and heat treatment. The investigation verified the effective energy transfer from $Er^{3+}$to Cr^{3+} in a Yb^{3+}/Er^{3+}/Cr^{3+} codoped precursor glass. During crystallization, the RE^{3+} and Cr^{3+} ions assimilated into the $NaYF_4$ and $NaAlSiO_4$ nanocrystals, isolating the ET between these ions. The fluorescence intensity ratio between $^4F_{7/2}/^4S_{3/2}$-$^4I_{9/2}$ and $^4F_{3/2}$-$^4I_{9/2}$ transitions of the Nd^{3+} ions in the range of 400 K–573 K and the FIR originating from the non-thermally coupled system of Cr-Nd. Due to Yb^{3+} being the only to absorb 980 nm photons, there is an energy imbalance between Yb^{3+}:^{2} $F^{5/2}$ and Nd^{3+}:$^4F^{3/2}$ energy states [160]. To produce near-infrared emissions from samples doped with Yb^{3+}/Er^{3+}/Cr^{3+}, phonon-assisted energy transfer from the thermal population and Yb^{3+} to Nd^{3+} ions is required due to this difference. When the emission spectra were compared, the latter had stronger emission peaks at 862 and 803 nm and a distinct peak at 750 nm. This mechanism is demonstrated in Figure 6(a). This Yb^{3+}/Er^{3+}/Cr^{3+} codoped oxyfluoride glass ceramic offers high-accuracy temperature measurement over a broad range, setting a new standard for optical temperature sensors [161].

Yao et al. synthesized $NaYF_4$: Er, Yb phosphors by incorporating varying concentrations of Mn through a solvothermal method. As the concentration of Mn doping improved, the sample size and morphology transitioned from large rod-like structures to smaller cubes. Excited by a 980 nm wavelength laser, all samples exhibited two distinct green emission bands centered at 527 and 549 nm, alongside a red emission band positioned at 649 nm, attributed to the transitions of $^2H_{11/2}$, $^4S_{3/2} \rightarrow ^4I_{15/2}$ and $^4F_{9/2} \rightarrow ^4I_{15/2}$, respectively. Particularly, the luminescence intensities of Mn-doped samples, notably in the red region, surpassed those of the 0% Mn sample [163]. The energy level diagram and the energy transfer processes were schematically represented in Figure 6(b).

Mn^{2+}ion was added, resulting in a nonradiative energy transfer between Mn^{2+} and Er^{3+}. This transfer involved back-energy flowing from the $^4T_1$ state of Mn^{2+} to the $^4F_{9/2}$ state of Er^{3+}, after which electrons from the $^2H_{9/2}$ and $^4S_{3/2}$ states of Er^{3+} moved to the $^4T_1$ state of Mn^{2+} [166]. As a result, this technique expedited red emission augmentation. The distance between Er^{3+} and Mn^{2+} significantly shrank as the concentration of Mn rose, encouraging a more active energy transfer process between both elements. This increased transmission enhanced the red emission. During temperature testing between 300 K and 30 K, the 20% Mn sample displayed a consistent and more pronounced increase in UC efficiency compared to the 0% Mn sample. This enhancement stemmed from the reduction of recombination centers due to decreasing temperature. Employing the FIR technique based on thermally coupled level transitions of the Er^{3+} ions, the maximum sensitivities were measured as 0.0036 K^{-1} for the 0% Mn sample and 0.0057 K^{-1} for the 20% Mn sample at 300 K. These findings collectively underscore the effectiveness of Mn doping in optimizing the sensitivity of fluorescence-based temperature sensors.

Cao et al. [165] highlighted a strong correlation between the UCL properties and the Nd^{3+} doping concentration and temperature. The observed enhancement of infrared upconversion in Nd^{3+} with rising temperature stemmed from effective energy transfer from Er^{3+} to Nd^{3+} ions validated through fluorescence kinetic analysis and energy rate equations. Exploiting the temperature-dependent UCL behavior, they iden-

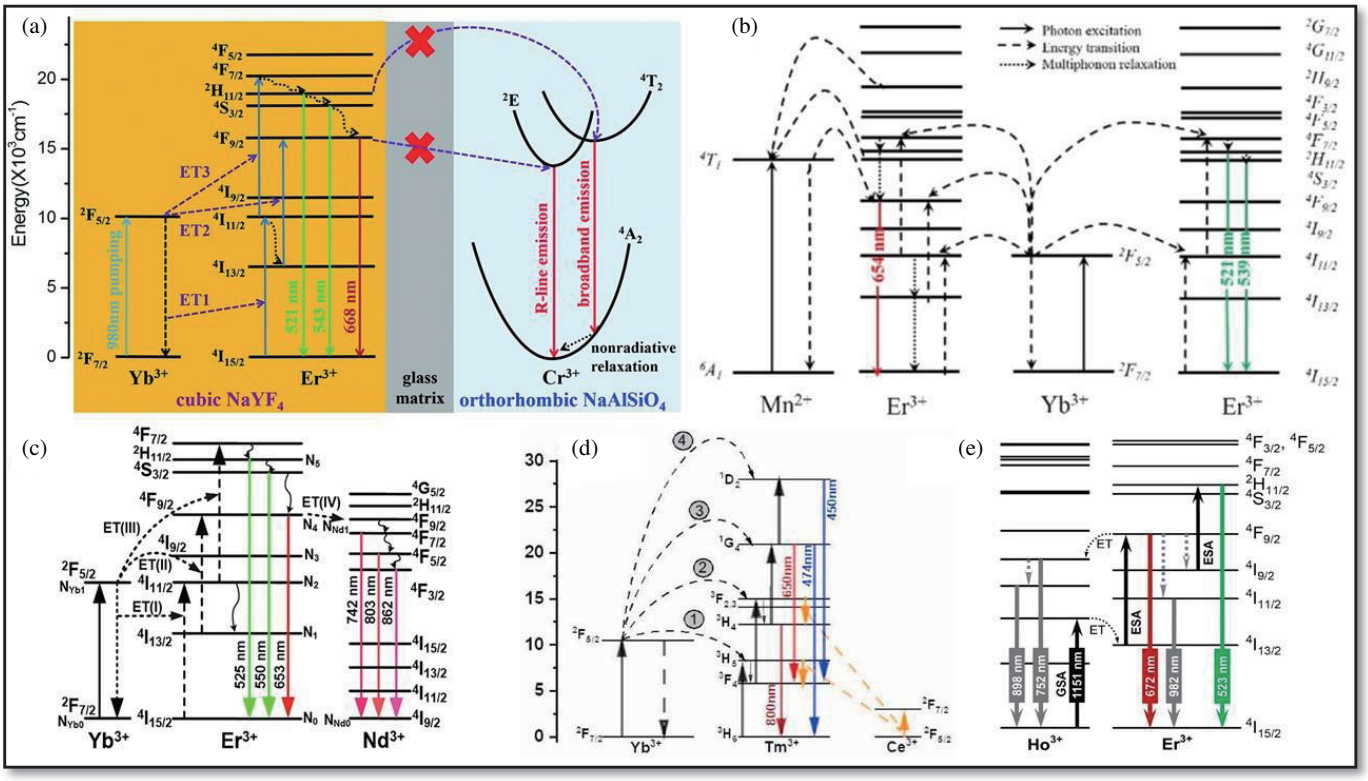

FIGURE 6. (a) describes a schematic energy level for the Er^{3+} and Cr^{3+} ions in a dual-phase Er-Cr system. (b) a schematic energy level diagram depicting the energy levels of Yb^{3+}, Er^{3+}, and Mn^{2+} ions. (c) the energy level diagram and potential energy transfer (ET) mechanisms in $NaYF_4$: Er/Yb/Nd nanocrystals (NCs) when stimulated at a wavelength of 980 nm. (d) the energy transfer UC mechanisms observed in Yb^{3+}/Tm^{3+} upconverting systems explore the potential influence of Ce^{3+} ions on energy distribution. (e) An energy level diagram for Ho and Er was observed at a wavelength of 1151 nm [161–165].

tified an exponential correlation between the fluorescence intensity ratio from the thermally coupled energy levels of Er^{3+}: $^2H_{11/2}/^4S_{3/2}$and Nd^{3+}: $^4F_{7/2}/^4F_{5/2}/^4F_{3/2}$ and inter-ion energy levels $^4F_{9/2}$ of Er^{3+} and $^4F_{7/2}/^4F_{5/2}/^4F_{3/2}$ of Nd^{3+} with temperature across both cryogenic and high-temperature ranges. The energy exchange phenomenon is demonstrated in Figure 6(c). The maximum sensitivity reached approximately $0.83\,K^{-1}$. This study proposes using Er^{3+}/Nd^{3+} co-doped phosphors in luminescent thermometry due to their broad temperature range coverage. Pilch-Wróbel et al. [162] examined the effect of Ce^{3+} codoping in luminescent $NaYF_4$ nanoparticles doped with Yb^{3+} and Tm^{3+}, showcasing notable variations in their emission intensity ratios across multiple wavelength transitions ($^1D_2 \rightarrow ^3F_4$ at 450 nm, $^1G_4 \rightarrow ^3H_6$ at 475 nm, $^1G_4 \rightarrow ^3F_4$ at 650 nm, and $^3H_4 \rightarrow ^3H_6$ at 800 nm) shown in Figure 6(d). Incorporating Ce^{3+} ions into the material led to a twofold enhancement in the 450/800, 470/800, and 650/800 luminescence intensity bands ratios (FIR). Modifying the excitation conditions and explicitly altering the pulse width resulted in a threefold increase in these FIR. The luminescence properties showed temperature dependency, revealing a relative sensitivity of approximately 4%/K for the 450/800 and 470/800 band ratios and close to 5.5%/K for the 650/800 band ratio around 0°C. However, as the temperature range shifted to physiological levels, the thermal sensitivity decreased to approximately 2%/K for the 450/800 and 470/800 bands ratios and above 2.5%/K for the 650/800 bands. $NaYF_4$:Ho^{3+}, Er^{3+}@$NaYF_4$ nanoparticles were meticulously synthesized via a controlled reaction in oleic acid and octadecene at 573 K. The spectroscopic properties of these products were extensively analyzed, focusing on the upconversion emission observed under 1151 nm laser excitation across a temperature range from 295 to 378 K. The sample doped with Ho^{3+} and Er^{3+} ions demonstrated a distinct behavior wherein the emission intensity increased with rising temperature. Most of the energy that Ho^{3+} ions absorb passes on to Er^{3+} ions, as shown in Figure 6(e). Exciting Er^{3+} ions to $^4F_{9/2}$ levels makes an extra emission possible, which results in a peak at 672 nm. After relaxation to the $^4I_{11/2}$ state, there is a strong emission at 982 nm. An extra emission band at 523 nm is produced when the Er^{3+} ion absorbs another photon, which populates the $^2H_{11/2}$ and $^4S_{3/2}$ levels of Er^{3+}. Though it is weaker than in a system with only Ho^{3+} ions, the emission from Ho^{3+} ions at 890 and 743 nm is caused by energy transfer from the excited Er^{3+} ions. This unique property showcased a relative sensitivity reaching its peak value of $1.80\%\,K^{-1}$ at 378 K. These findings underscore the exceptional optical temperature sensing capabilities of the $NaYF_4$:Ho^{3+}, Er^{3+}@$NaYF_4$ system, mainly relying on the luminescence intensity ratios of the near-infrared bands associated with both Ho^{3+} and Er^{3+} ions [164].

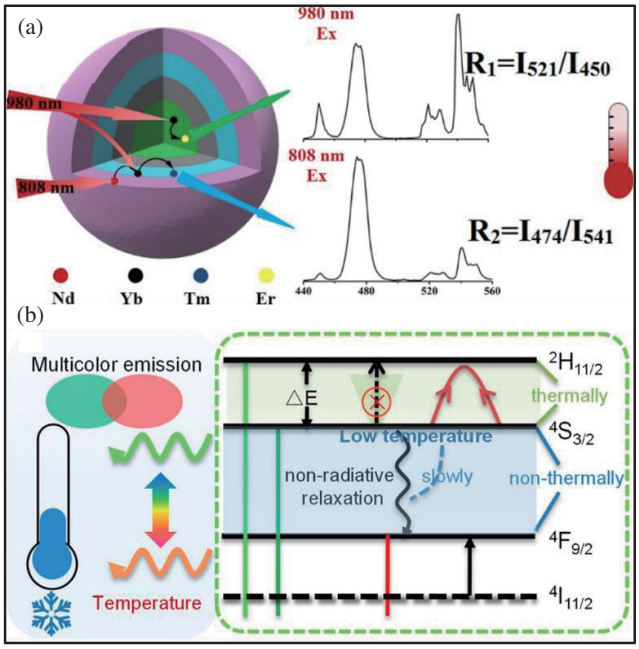

FIGURE 7. (a) illustrates the schematic diagram of a temperature sensor system utilizing Erbium (Er), Yttrium (Y), Thulium (Tm), and Neodymium (Nd) ions. The system operates under the stimulation of two different wavelengths. (b) schematic illustration diagram depicting the thermally coupled levels ($^2H_{11/2}$, $^4S_{3/2}$) and nonthermally coupled levels ($^4F_{9/2}$, $^4S_{3/2}$) that contribute to the emission of many colors [167, 169].

15. FIR BETWEEN THERMALLY NON-COUPLED LEVELS

The lack of correlation between the temperature dependence of the two different emissions and the energy transfer between the two excited states is demonstrated. These mechanisms are relevant in cases where temperature does not impact energy transfer between the two excited states. Ba et al. [167] developed multilayer core-shell-shell-shell nanoparticles, denoted as $NaYF_4$:Yb,Er@ $NaYF_4$@$NaYF_4$:Yb,Tm@ $NaYF_4$:Nd, tailored for high-sensitivity non-contact fluorescence nanothermometry which is shown in Figure 7(a). These nanoparticles integrated distinct fluorescence centers, Er^{3+} and Tm^{3+}, strategically positioned in separate regions within the nanostructure and isolated by a $NaYF_4$ barrier to prevent energy cross-relaxation. The addition of Nd^{3+} doping in the outermost layer enabled robust fluorescence performance upon excitation at 808 nm. Notably, results obtained using 980 nm excitation indicated its potential as a dual-wavelength-stimulated thermal probe. Specifically, the luminescence intensity exhibited explicit temperature-dependent behavior within the physiological temperature range. The intensity ratio, representing a quadratic function with temperature, demonstrated improved sensitivity by considering emissions from different ions situated in distinct layers, contrasting those emanating from the same ions. The sensitivity enhanced significantly, reaching maximum values of 2.95% K^{-1} and 6.30% K^{-1} when excited at 980 nm and 808 nm, respectively. This pioneering approach, employing a multilayer core-shell-shell-shell structure with varied ion doping across layers and leveraging non-thermally coupled fluorescence intensities, presents a promising strategy to enhance the sensitivity of temperature sensors substantially. The first author's group has studied a wide-range thermal sensing method, relying on the two-photon upconversion luminescence of the high-temperature cubic phase $NaYF_4$:Yb, Er. Through temperatures ranging from room temperature to 973 K, the single-phase sample demonstrates two distinct emission bands in green and red, each showcasing different temperature dependencies. Using the CIE chromaticity diagram to look at the data shows an apparent change in the color point trajectory, going from a deep red color (0.6357, 0.3501) at room temperature to a yellow region (0.4379, 0.475) at 600 K and then to a green region (0.318, 0.669) at 973 K. This shift indicates the potential of HT cubic-phase $NaYF_4$:Yb, Er as a promising ratiometric and colorimetric luminescent thermometer. The study reveals a nuanced trend in relative sensitivity across the temperature range. Up to 673 K, there is a slight decrease in sensitivity, then an increase as the temperature rises. The enlargement of the lattice in the high-temperature cubic phase has a substantial impact on the crystal symmetry surrounding the activator ion. This change strengthens the green-to-red emission ratio, which helps explain why luminescence behaves differently at different temperatures [168]. Nie et al. achieved multicolor upconversion luminescence by leveraging unique cryogenic-dependent energy manipulation. Their research gives us a new way to think about how green emissions work when excited by 1550 nm light, especially in a cryogenic system. They highlight that the electrons at the $^2H_{11/2}$ level predominantly originate from the $^4S_{3/2}$ level. Their research is mainly about a substance that has Er^{3+} ions added to it. It works on levels that are not thermally coupled ($^4F_{9/2}$ and $^4S_{3/2}$) and gives off different colors of light when it cools down [169]. The scheme is demonstrated in Figure 7(b).

TABLE 1. Thermometry data comparison of dual-mode luminescence materials using the FIR technique, listing Lanthanide dopant, excitation wavelength, temperature range (K), maximum sensitivity, and temperature resolution.

Lanthanide	Excitation wavelength	Temp. range (K)	Max Sr $(K)^{-1}$	At temp. (K)	Temperature resolution	Ref.
Yb, Nd	880	223–473	16.9	223	0.1–0.2	[159]
Yb. Er	980	304–321	1.1	304	0.08–0.09	[171]
Nd	808	318–327	1.0	318	0.28–0.30	[171]
Yb. Er	980	300–900	1.02	300	0.2–0.3	[153]
Er, Yb, Nd	980	298-413	9.6 2.3	298 413	< 1	[156]
Yb, nd, tm	808	285–345 345–495	0.88 1.89	285–345 345–495		[172]
Tm. Yb	980	303–423	2.13	303		[173]
Yb, Nd	808	150–450	2.10	370		[174]
Yb, Er	980	293–373	1.62	293		[175]
Yb, Er	975	299–337	1.31	299	0.59–1.0	[155]
Er, Tm	980	298–503	2.61	298		[176]
Yb, Er, Nd, Tm	980	313–553	23.84	380		[157]
Er	980	298–348	30.2	298		[158]
Ho, Er	1151	295–378	1.80	378		[164]
Yb, Ho, Tm	980	300–500	1.796	345	0.0167	[170]
Er	1550	100–350	4.225	150		[169]

This research establishes high sensitivity, enabling the development of temperature measurements through visual reading and digital recognition. These results help us learn more about how UC luminescence changes and give us valuable ideas for making materials that can sense temperature in many colors. A series of $NaYF_4$:Yb^{3+}/Ho^{3+} upconversion green phosphors co-doped with varying concentrations of Mg^{2+}/Sc^{3+} were synthesized. The study used fluorescence intensity ratios (FIR) to determine its sensitivity, focusing on the levels ($^5F_5$/$^5F_4$, $^5S_2$) of Ho^{3+} ions that are not thermally coupled. The optimized phosphor displayed maximum sensitivity values, with Sa reaching 0.00119 K^{-1} at 574 K and Sr at 0.258% K^{-1} at 374 K. Also, the upconversion emission intensity stayed stable, keeping about 65% of its intensity at 423 K and 36% at 574 K, compared to room temperature. This retention highlights the thermal stability of the phosphors for their potential for applications in environments with varying temperatures.

Cheng et al. fabricate hexagonal phase $NaYF_4$:Yb^{3+}/Ho^{3+}/Tm^{3+} nanoparticles. The study delved into evaluating the responsiveness of various energy levels to temperature variations using FIR techniques, focusing on Thermally Coupled Levels (TCLs) and Non-Thermally Coupled Levels (NTCLs). Notably, a significant temperature-dependent FIR was observed, with NTCLs exhibiting an impressive fit above 99.5%. The experimental findings underscored the exceptional performance of Ho^{3+}/Tm^{3+}/Yb^{3+} triple-doped $NaYF_4$ as an optical temperature sensing medium. The material had excellent temperature-sensing properties. Its highest absolute sensitivity (Sa), lowest relative sensitivity (Sr), and highest temperature resolution based on NTCLs were 0.0126 K^{-1} at 495 K, 1.7966% K^{-1} at 345 K, and 0.0167 K, respectively. These values far surpassed those of most optical sensing materials. Additionally, the distinct emission bands of NTCLs provided excellent discrimination in temperature-sensing signals. The material exhibited enhanced sensory capabilities due to the synergistic interplay of non-radiative relaxation, thermal excitation, and energy transfer mechanisms throughout the heating process. This synergy between these factors underscored the remarkable temperature-sensing performance of the Ho^{3+}/Tm^{3+}/Yb^{3+} triple-doped $NaYF_4$, positioning it as a promising material in optical temperature-sensing applications. Thermally coupled levels showcase exceptional accuracy and sensitivity across a wide temperature spectrum [170]. A comparative analysis is presented in Table 1, detailing essential thermometric parameters of dual-mode luminescence materials utilizing the FIR technique with various Lanthamide dopants.

Research highlights high-precision temperature measurements achievable via distinct fluorescence centers and multilayer nanostructures, enabling enhanced sensitivity within physiological temperature ranges. These methods offer promising avenues for precise temperature sensing in biological and biomedical applications. Additionally, investigations into multicolor upconversion luminescence and sensitivity enhancements from thermally non-coupled levels demonstrate unique cryogenic-responsive emissions and the development of high-sensitivity, multicolor temperature-sensing materials. These studies present innovative approaches for temperature measurement, potentially expanding applications across

diverse environments and temperature ranges. In summary, the thermometric results from these studies underscore the versatility and potential of fluorescence intensity ratios based on optical temperature sensing methods. These findings showcase remarkable accuracy, sensitivity, and adaptability, laying a robust foundation for advancing precision temperature measurements in scientific, biomedical, and technological domains.

16. CONCLUSION AND PERSPECTIVES

This review provided an overview of the latest advancements in lanthanide-doped $NaYF_4$. Initially, the primary focus of the research was on synthesizing high-quality UCNPs. This was achieved by manipulating several factors, such as the types and concentrations of doping ions, particle size, phase, host materials, and the introduction of non-rare earth ions or metal nanoparticles. A comprehensive examination was conducted on various methods to achieve controlled synthesis of lanthanide-doped nano/microcrystals of $NaYF_4$. The adjustment of precursor and synthesis parameters has produced a diverse range of high-quality nanocrystals with customized morphologies. However, the existing control procedures heavily rely on experimental trial-and-error methods. Simultaneously, most synthetic processes are comprised of hypotheses due to the absence of a reliable measuring approach and validating evidence. Hence, there is a pressing need to create a monitoring technique to understand the reaction process's underlying mechanism. Furthermore, enhanced comprehension of synthetic methods would facilitate the systematic development of synthetic strategies, guiding the production of nano/microcrystals with preconceived architectures. In the meantime, much research has been done on making superior lanthanide-doped $NaYF_4$ UCNPs with a limited size distribution and strong luminescence efficiency. The exploration of novel upconversion ions, combinations of ions, and host materials continues to be a very active area of investigation.

Researchers who persist in their endeavours should employ suitable strategies for the synthesis of $NaYF_4$ nanoparticles doped with lanthanides to achieve the required size distribution and optical characteristics. Additionally, establishing efficient channels for energy transfer between these materials, designing structures to safeguard the emitting sites, and manipulating the matrix materials should also be pursued.

The diverse range of applications in which there is a demand for nanoscale temperature sensors requires the creation of a comprehensive collection of temperature sensors that demonstrate exceptional performance in several complementing aspects. Instead of emphasizing particular applications, this paper aims to elucidate the photophysical mechanisms that underlie the dual emission observed in different optical temperature sensors, enabling ratiometric detection. The diverse agents have been exemplified through contemporary literature. A sensitivity meter has been established with a specific focus on dual-emitting sensors, allowing for quantitative evaluation and comparison of these sensors. Additionally, the constraints and drawbacks associated with these metrics have been addressed in the discussion. The recent identification of a novel dual-emission phenomenon in nanocrystals doped with Mn^{2+}, Ce^{+2} ions, etc., has garnered significant attention. It has resulted in the development of a novel category of nanothermometers that exhibit exceptional characteristics in terms of adjustability, sensitivity, luminosity, and accuracy in measuring temperature. These attributes make them suitable for various demanding applications in optical nanothermometry.

When considering the particular use of temperature sensors, numerous materials used in FIR thermometers have also faced certain obstacles. The object's temperature to be measured may be influenced by the photo-thermal effect of the excitation of 980 nm light. Furthermore, the specifications for thermometers vary across various temperature measuring settings. Thermometers for detecting minute temperature variations in biologically active tissues or cells necessitate a high level of sensitivity within a limited physiological temperature range. The successful operation of temperature detection requires using thermometer materials with exceptional optical thermal stability, enabling them to function effectively in elevated temperature conditions. Consequently, it is imperative to establish precise standards for thermometers to give researchers a reliable reference point. In conclusion, the FIR thermometer is anticipated to progress in enhanced sensitivity, improved resolution, and expanded temperature range. Consequently, the FIR thermometer is expected to find extensive application across diverse temperature sensing scenarios in the foreseeable future.

The utilization of UCNPs in thermometry and STED microscopy presents a promising avenue for enhancing imaging modalities. Their unique optical properties allow for nanoscale temperature detection and the prospect of surpassing the resolution limitations inherent in conventional microscopy techniques. In thermometry, UCNPs exhibit sensitivity to temperature alterations by altering the emitted light's intensity ratio, enabling precise temperature mapping at cellular and sub-cellular levels. This characteristic makes them valuable candidates for probing localized thermal changes within biological systems. Moreover, in STED microscopy, UCNPs hold potential as contrast agents owing to their distinctive spectral features and photostability. The integration of UCNPs could augment resolution capabilities, enabling sharper imaging of minute cellular structures beyond the diffraction limit.

ACKNOWLEDGEMENT

This work is partially supported by the "Pioneer" and "Leading Goose" R&D Program of Zhejiang (No. 2023C03002, 2023C03083, and 2023C03135), the National Key Research and Development Program of China (No. 2022YFC2010000 and 2022YFC3601002) and the National Natural Science Foundation of China (No. 11621101).

REFERENCES

[1] Xu, C. T., Q. Zhan, H. Liu, G. Somesfalean, J. Qian, S. He, and S. Andersson-Engels, "Upconverting nanoparticles for preclinical diffuse optical imaging, microscopy and sensing: current trends and future challenges," *Laser & Photonics Reviews*, Vol. 7, No. 5, 663–697, Sep. 2013.

[2] Wang, D., J. Qian, F. Cai, S. He, S. Han, and Y. Mu, "'Green'-synthesized near-infrared Pbs quantum dots with silica-PEG dual-layer coating: ultrastable and biocompatible optical probes for in vivo animal imaging," *Nanotechnology*, Vol. 23, No. 24, Jun. 2012.

[3] Zhan, Q., H. Cheng, J. Qian, and S. He, "Multi-photon evanescent wave (MPEW) excited lanthanide-doped upconverting nanoparticles (UCNPs) for fast single particles tracking and live cell membrane imaging," in *Asia Communications and Photonics Conference*, AS3E–3, 2012.

[4] Liu, J., R. Wu, N. Li, X. Zhang, Q. Zhan, and S. He, "Deep, high contrast microscopic cell imaging using three-photon luminescence of β-($NaYF_4$:Er^{3+}/$NaYF_4$) nanoprobe excited by 1480-nm CW laser of only 1.5-mW," *Biomedical Optics Express*, Vol. 6, No. 5, 1857–1866, 2015.

[5] Qian, J., L. Jiang, F. Cai, D. Wang, and S. He, "Fluorescence-surface enhanced raman scattering co-functionalized gold nanorods as near-infrared probes for purely optical in vivo imaging," *Biomaterials*, Vol. 32, No. 6, 1601–1610, Feb. 2011.

[6] Qian, J., D. Wang, F.-H. Cai, W. Xi, L. Peng, Z.-F. Zhu, H. He, M.-L. Hu, and S. He, "Observation of multiphoton-induced fluorescence from graphene oxide nanoparticles and applications in in vivo functional bioimaging," *Angewandte Chemie-international Edition*, Vol. 51, No. 42, 10 570–10 575, 2012.

[7] Wang, S., X. Zhao, S. Wang, J. Qian, and S. He, "Biologically inspired polydopamine capped gold nanorods for drug delivery and light-mediated cancer therapy," *ACS Applied Materials & Interfaces*, Vol. 8, No. 37, 24 368–24 384, Sep. 2016.

[8] Zhan, Q., B. Wang, X. Wen, and S. He, "Controlling the excitation of upconverting luminescence for biomedical theranostics: neodymium sensitizing," *Optical Materials Express*, Vol. 6, No. 4, 1011–1023, Apr. 2016.

[9] Zhan, Q., J. Qian, H. Liang, G. Somesfalean, and S. Andersson-Engels, "Using 915 nm laser excited Tm^{3+}/Er^{3+}/Ho^{3+}-doped $NaYbF_4$ upconversion nanoparticles for in vitro and deeper in vivo bioimaging without overheating irradiation," *ACS Nano*, Vol. 5, No. 5, 3744–3757, 2011.

[10] Zhan, Q., S. He, J. Qian, H. Cheng, and F. Cai, "Optimization of optical excitation of upconversion nanoparticles for rapid microscopy and deeper tissue imaging with higher quantum yield," *Theranostics*, Vol. 3, No. 5, 306–316, 2013.

[11] Wang, S., X. Zhao, J. Qian, and S. He, "Polyelectrolyte coated $BaTiO_3$ nanoparticles for second harmonic generation imaging-guided photodynamic therapy with improved stability and enhanced cellular uptake," *RSC Advances*, Vol. 6, No. 46, 40 615–40 625, 2016.

[12] Sun, X., Z. Ji, and S. He, "SHG-enhanced NIR-excited in vitro photodynamic therapy using composite nanoparticles of barium titanate and rose bengal," *RSC Advances*, Vol. 9, No. 14, 8056–8064, 2019.

[13] Li, N., X. Wen, J. Liu, B. Wang, Q. Zhan, and S. He, "Yb^{3+}-enhanced UCNP@SiO_2 nanocomposites for consecutive imaging, photothermal-controlled drug delivery and cancer therapy," *Optical Materials Express*, Vol. 6, No. 4, 1161–1171, 2016.

[14] Qian, J., D. Wang, F. Cai, Q. Zhan, Y. Wang, and S. He, "Photosensitizer encapsulated organically modified silica nanoparticles for direct two-photon photodynamic therapy and functional imaging," *Biomaterials*, Vol. 33, No. 19, 4851–4860, Jun. 2012.

[15] Sun, X., A. Zebibula, X. Dong, G. Li, G. Zhang, D. Zhang, J. Qian, and S. He, "Targeted and imaging-guided in vivo photodynamic therapy for tumors using dual-function, aggregation-induced emission nanoparticles," *Nano Research*, Vol. 11, No. 5, 2756–2770, May 2018.

[16] Wang, B., Q. Zhan, Y. Zhao, R. Wu, J. Liu, and S. He, "Visible-to-visible four-photon ultrahigh resolution microscopic imaging with 730-nm diode laser excited nanocrystals," *Optics Express*, Vol. 24, No. 2, A302–A311, Jan. 2016.

[17] Zhan, Q., H. Liu, B. Wang, Q. Wu, R. Pu, C. Zhou, B. Huang, X. Peng, H. Gren, and S. He, "Achieving high-efficiency emission depletion nanoscopy by employing cross relaxation in upconversion nanoparticles," *Nature Communications*, Vol. 8, Oct. 2017.

[18] Wu, R., Q. Zhan, H. Liu, X. Wen, B. Wang, and S. He, "Optical depletion mechanism of upconverting luminescence and its potential for multi-photon STED-like microscopy," *Optics Express*, Vol. 23, No. 25, 32 401–32 412, Dec. 2015.

[19] Zhao, Y., Q. Zhan, J. Liu, and S. He, "Optically investigating Nd^{3+}-Yb^{3+} cascade sensitized upconversion nanoparticles for high resolution, rapid scanning, deep and damage-free bioimaging," *Biomedical Optics Express*, Vol. 6, No. 3, 838–848, 2015.

[20] Zhang, G., H. Dong, D. Wang, L. Sun, and C. Yan, "Investigations on multi-photon emissions of Nd^{3+}-sensitized core/shell nanoparticles," *Journal of Rare Earths*, 2017.

[21] Bi, X., G. He, W. Di, and W. Qin, "Enhanced near-infrared upconversion luminescence of Na_4YFYb^{3+}, Tm^{3+}/CdSe nanoheterostructures," *Materials Letters*, Vol. 173, 187–190, Jun. 2016.

[22] Shao, B., Y. Feng, Y. Song, M. Jiao, W. Lü, and H. You, "Topotactic transformation route to monodisperse β-$NaYF_4$:Ln^{3+} microcrystals with luminescence properties," *Inorganic Chemistry*, Vol. 55, No. 4, 1912–1919, 2016.

[23] Li, J., G. Hu, L. Shi, N. He, D. Li, Q. Shang, Q. Zhang, H. Fu, L. Zhou, W. Xiong, J. Guan, J. Wang, S. He, and L. Chen, "Full-color enhanced second harmonic generation using rainbow trapping in ultrathin hyperbolic metamaterials," *Nature Communications*, Vol. 12, No. 1, Nov. 2021.

[24] Xia, J., J. Tang, F. Bao, Y. Sun, M. Fang, G. Cao, J. Evans, and S. He, "Turning a hot spot into a cold spot: polarization-controlled fano-shaped local-field responses probed by a quantum dot," *Light-Science & Applications*, Vol. 9, No. 1, Sep. 2020.

[25] Shao, B., Z. Yang, J. Li, J. Yang, Y. Wang, J. Qiu, and Z. Song, "Upconversion emission enhancement by porous silver films with ultra-broad plasmon absorption," *Optical Materials Express*, Vol. 7, No. 4, 1188–1197, Apr. 2017.

[26] Gong, C., W. Liu, N. He, H. Dong, Y. Jin, and S. He, "Upconversion enhancement by a dual-resonance all-dielectric metasurface," *Nanoscale*, Vol. 11, No. 4, 1856–1862, Jan. 2019.

[27] Hu, Z., N. He, Y. Sun, Y. Jin, and S. He, "Wideband high-reflection chiral dielectric metasurface," *Progress In Electromagnetics Research*, Vol. 172, 51–60, 2021.

[28] Zhan, Q., X. Zhang, Y. Zhao, J. Liu, and S. He, "Tens of thousands-fold upconversion luminescence enhancement induced by a single gold nanorod," *Laser & Photonics Reviews*, Vol. 9, No. 5, 479–487, Sep. 2015.

[29] Wu, N., Y. Zhang, H. Ma, H. Chen, and H. Qian, "Tunable high-Q plasmonic metasurface with multiple surface lattice resonances," *Progress In Electromagnetics Research*, Vol. 172, 23–32, 2021.

[30] Hu, S., S. Wu, C. Li, R. Chen, E. Forsberg, and S. He, "SNR-enhanced temperature-insensitive microfiber humidity sensor based on upconversion nanoparticles and cellulose liquid crystal coating," *Sensors and Actuators B-chemical*, Vol. 305, Feb. 2020.

[31] Zhang, H., J. Sun, J. Yang, I. D. Leon, R. P. Zaccaria, H. Qian, H. Chen, G. Wang, and A. Wang, "Biosensing performance of a plasmonic-grating-based nanolaser," *Prog. Electromagn. Res*, Vol. 171, 159–169, 2021.

[32] Liu, W., R. Chen, and S. He, "Ultra-stable near-infrared Tm^{3+}-doped upconversion nanoparticles for wide-field two-photon angiography with a low excitation intensity," *Journal of Innovative Optical Health Sciences*, Vol. 12, No. 3, May 2019.

[33] Ding, F., "A review of multifunctional optical gap-surface plasmon metasurfaces," *Progress In Electromagnetics Research*, Vol. 174, 55–73, 2022.

[34] Xu, C. T., Q. Zhan, H. Liu, G. Somesfalean, J. Qian, S. He, and S. Andersson-Engels, "Upconverting nanoparticles for preclinical diffuse optical imaging, microscopy and sensing: Current trends and future challenges," *Laser & Photonics Reviews*, Vol. 7, No. 5, 663–697, Sep. 2013.

[35] Cai, F. and S. He, "Electric field Monte Carlo simulation of focused stimulated emission depletion beam, radially and azimuthally polarized beams for in vivo deep bioimaging," *Journal of Biomedical Optics*, Vol. 19, No. 1, 11022, Jan. 2014.

[36] Ploschner, M., D. Denkova, S. D. Camillis, M. Das, L. M. Parker, X. Zheng, Y. Lu, S. Ojosnegros, and J. A. Piper, "Simultaneous super-linear excitation-emission and emission depletion allows imaging of upconversion nanoparticles with higher sub-diffraction resolution," *Optics Express*, Vol. 28, No. 16, 24 308–24 326, Aug. 2020.

[37] Liu, Y., Y. Lu, X. Yang, X. Zheng, S. Wen, F. Wang, X. Vidal, J. Zhao, D. Liu, Z. Zhou, C. Ma, J. Zhou, J. A. Piper, P. Xi, and D. Jin, "Amplified stimulated emission in upconversion nanoparticles for super-resolution nanoscopy," *Nature*, Vol. 543, No. 7644, 229–233, Mar. 2017.

[38] De Camillis, S., P. Ren, Y. Cao, M. Ploschner, D. Denkova, X. Zheng, Y. Lu, and J. A. Piper, "Controlling the nonlinear emission of upconversion nanoparticles to enhance super-resolution imaging performance," *Nanoscale*, Vol. 12, No. 39, 20 347–20 355, Oct. 2020.

[39] Tian, Y., Y. Tian, P. Huang, L. Wang, Q. Shi, and C. Cui, "Effect of Yb^{3+} concentration on upconversion luminescence and temperature sensing behavior in Yb^{3+}/Er^{3+} co-doped $YNbO_4$ nanoparticles prepared via molten salt route," *Chemical Engineering Journal*, Vol. 297, 26–34, Aug. 2016.

[40] Zhao, J., X. Zheng, E. P. Schartner, P. Ionescu, R. Zhang, T.-L. Nguyen, D. Jin, and H. Ebendorff-Heidepriem, "Glass fibers: upconversion nanocrystal-doped glass: A new paradigm for photonic materials (advanced optical materials 10/2016)," *Advanced Optical Materials*, Vol. 4, No. 10, 1419–1419, 2016.

[41] Kim, S., S.-H. Hwang, S.-G. Im, M.-K. Lee, C.-H. Lee, S. J. Son, and H.-B. Oh, "Upconversion nanoparticle-based forster resonance energy transfer for detecting DNA methylation," *Sensors*, Vol. 16, No. 8, Aug. 2016.

[42] He, M., X. Pang, X. Liu *et al.*, "Innenrucktitelbild: monodisperse dual-functional upconversion nanoparticles enabled near-infrared organolead halide perovskite solar cells (Angew. Chem. 13/2016)," *Angewandte Chemie*, Vol. 55, No. 13, Mar. 2016.

[43] Shangguan, M., H. Xia, C. Wang, J. Qiu, G. Shentu, Q. Zhang, X. Dou, and J.-W. Pan, "All-fiber upconversion high spectral resolution wind lidar using a Fabry-Perot interferometer," *Optics Express*, Vol. 24, No. 17, 19 322–19 336, Aug. 2016.

[44] Liu, Y., N. Kang, J. Lv, Z. Zhou, Q. Zhao, L. Ma, Z. Chen, L. Ren, and L. Nie, "Deep photoacoustic/luminescence/magnetic resonance multimodal imaging in living subjects using high-efficiency upconversion nanocomposites," *Advanced Materials*, Vol. 28, No. 30, 6411–6419, Aug. 2016.

[45] Gu, Z., L. Yan, G. Tian, S. Li, Z. Chai, and Y. Zhao, "Recent advances in design and fabrication of upconversion nanoparticles and their safe theranostic applications," *Advanced Materials*, Vol. 25, No. 28, 3758–3779, 2013.

[46] Park, W., D. Lu, and S. Ahn, "Plasmon enhancement of luminescence upconversion," *Chemical Society Reviews*, Vol. 44, No. 10, 2940–2962, 2015.

[47] Shao, B., Q. Zhao, Y. Jia, W. Lv, and M. a. Jiao, "A novel synthetic route towards monodisperse β-$NaYF_4$: Ln^{3+} micro/nanocrystals from layered rare-earth hydroxides at ultra low temperature," *Chem. Commun.*, Vol. 50, No. 84, 12 706–12 709, Aug. 2014.

[48] Zhou, B., B. Shi, D. Jin, and X. Liu, "Controlling upconversion nanocrystals for emerging applications," *Nature Nanotechnology*, Vol. 10, No. 11, 924–936, Nov. 2015.

[49] Thoma, R. E., G. M. Hebert, H. Insley, and C. F. Weaver, "Phase equilibria in the system sodium fluoride-yttrium fluoride," *Inorganic Chemistry*, Vol. 2, No. 5, 1005–1012, 1963.

[50] Du, P., J. Tang, W. Li, and L. Luo, "Exploiting the diverse photoluminescence behaviors of NaLuF4:xEu^{3+} nanoparticles and g-C3N4 to realize versatile applications in white light-emitting diode and optical thermometer," *Chemical Engineering Journal*, Vol. 406, Feb. 2021.

[51] Baride, A., P. S. May, and M. T. Berry, "Cross-relaxation from Er^{3+} ($^2H_{11/2}$, $^4S_{3/2}$) and Er^{3+} ($^2H_{9/2}$) in β-$NaYF_4$:Yb, Er and implications for modeling upconversion dynamics," *The Journal of Physical Chemistry C*, Vol. 124, No. 3, 2193–2201, 2019.

[52] Wang, H.-Q., M. Batentschuk, A. Osvet, L. Pinna, and C. J. Brabec, "Rare-earth ion doped up-conversion materials for photovoltaic applications," *Advanced Materials*, Vol. 23, No. 22-23, 2675–2680, Jun. 2011.

[53] Chen, Z., H. Chen, H. Hu, M. Yu, F. Li, Q. Zhang, Z. Zhou, T. Yi, and C. Huang, "Versatile synthesis strategy for carboxylic acid-functionalized upconverting nanophosphors as biological labels," *Journal of The American Chemical Society*, Vol. 130, No. 10, 3023–3029, Mar. 2008.

[54] Eliseeva, S. V. and J.-C. G. Buenzli, "Lanthanide luminescence for functional materials and bio-sciences," *Chemical Society Reviews*, Vol. 39, No. 1, 189–227, 2010.

[55] Zhang, H., Z. Yang, Y. Wang, Y. Ma, J. Qiu, and Z. Song, "Near infrared light-induced photocurrent in $NaYF_4$:Yb^{3+}, Er^{3+}/$WO_{2.72}$ composite film," *Journal of The American Ceramic Society*, Vol. 103, No. 3, 1677–1684, 2020.

[56] Zeng, J.-H., J. Su, Z.-H. Li, R.-X. Yan, and Y.-D. Li, "Synthesis and upconversion luminescence of hexagonal-phase $NaYF_4$:Yb, Er^{3+} phosphors of controlled size and morphology," *Advanced Materials*, Vol. 17, No. 17, 2119–2123, 2005.

[57] Ding, M., S. Yin, D. Chen, J. Zhong, Y. Ni, C. Lu, Z. Xu, and Z. Ji, "Hexagonal $NaYF_4$:Yb^{3+}/Er^{3+} nano/micro-structures: controlled hydrothermal synthesis and morphology-dependent upconversion luminescence," *Applied Surface Science*, Vol. 333, 23–33, Apr. 2015.

[58] Ding, M., S. Yin, Y. Ni, C. Lu, D. Chen, J. Zhong, Z. Ji, and Z. Xu, "Controlled synthesis of β-$NaYF_4$:Yb^{3+}/Er^{3+} microstructures with morphology- and size-dependent upconversion luminescence," *Ceramics International*, Vol. 41, No. 6, 7411–7420, Jul. 2015.

[59] Dong, C., A. Korinek, B. Blasiak, B. Tomanek, and F. C. J. M. van Veggel, "Cation exchange: a facile method to make $NaYF_4$:Yb, Tm-$NaGdF_4$ core-shell nanoparticles with a thin, tunable, and uniform shell," *Chemistry of Materials*, Vol. 24,

No. 7, 1297–1305, 2012.

[60] Peng, J., Y. Sun, L. Zhao, Y. Wu, W. Feng, Y. Gao, and F. Li, "Polyphosphoric acid capping radioactive/upconverting $NaYF_4$:Yb,Tm,153Sm nanoparticles for blood pool imaging in vivo," *Biomaterials*, Vol. 34, No. 37, 9535–9544, Dec. 2013.

[61] Tu, D., Y. Liu, H. Zhu, and X. Chen, "Optical/magnetic multimodal bioprobes based on lanthanide-doped inorganic nanocrystals," *Chemistry — A European Journal*, Vol. 19, No. 18, 5516–5527, Apr. 2013.

[62] Wang, Y.-F., G.-Y. Liu, L.-D. Sun, J.-W. Xiao, J.-C. Zhou, and C.-H. Yan, "Nd^{3+}-sensitized upconversion nanophosphors: Efficient in vivo bioimaging probes with minimized heating effect," *ACS Nano*, Vol. 7, No. 8, 7200–7206, Aug. 2013.

[63] Xi, J., M. Ding, J. Dai, Y. Pan, D. Chen, and Z. Ji, "Comparison of upconversion luminescent properties and temperature sensing behaviors of β-$NaYF_4$:Yb^{3+}/Er^{3+} nano/microcrystals prepared by various synthetic methods," *Journal of Materials Science: Materials in Electronics*, Vol. 27, No. 8, 8254–8270, Aug. 2016.

[64] Ring, E. F. J., "The historical development of temperature measurement in medicine," *Infrared Physics & Technology*, Vol. 49, No. 3, 297–301, Jan. 2007.

[65] Weaver, J. B., "Bioimaging hot nanoparticles light up cancer," *Nature Nanotechnology*, Vol. 5, No. 9, 630–631, Sep. 2010.

[66] Wu, X., S. Wu, X. Chen, H. Lin, E. Forsberg, and S. He, "An ultra-compact and reproducible fiber tip michelson interferometer for high-temperature sensing," *Progress In Electromagnetics Research*, Vol. 172, 89–99, 2021.

[67] Wang, X., Q. Liu, Y. Bu, C.-S. Liu, T. Liu, and X. Yan, "Optical temperature sensing of rare-earth ion doped phosphors," *RSC Advances*, Vol. 5, No. 105, 86 219–86 236, 2015.

[68] Allison, S. W. and G. T. Gillies, "Remote thermometry with thermographic phosphors: instrumentation and applications," *Review of Scientific Instruments*, Vol. 68, No. 7, 2615–2650, Jul. 1997.

[69] Kamma, I., P. Kommidi, and B. R. Reddy, "Design of a high temperature sensing system using luminescence lifetime measurement," *Review of Scientific Instruments*, Vol. 79, No. 9, Sep. 2008.

[70] Feng, Z., S. Yang, H. Xia, C. Wang, D. Jiang, J. Zhang, X. Gu, Y. Zhang, B. Chen, and H. Jiang, "Energy transfer and 2.0 μm emission in Tm^{3+}/Ho^{3+} co-doped α-$NaYF_4$ single crystals," *Materials Research Bulletin*, Vol. 76, 279–283, 2016.

[71] Alden, M., A. Omrane, M. Richter, and G. Sarner, "Thermographic phosphors for thermometry: A survey of combustion applications," *Progress in Energy and Combustion Science*, Vol. 37, No. 4, 422–461, Aug. 2011.

[72] Fischer, L. H., G. S. Harms, and O. S. Wolfbeis, "Upconverting nanoparticles for nanoscale thermometry," *Angewandte Chemie-international Edition*, Vol. 50, No. 20, 4546–4551, 2011.

[73] Lee, J. K. and J. C. Kim, "Progenitor cells in healing after pterygium excision," *Yonsei Medical Journal*, Vol. 48, No. 1, 48–54, Feb. 2007.

[74] Jaque, D. and F. Vetrone, "Luminescence nanothermometry," *Nanoscale*, Vol. 4, No. 15, 4301–4326, 2012.

[75] Kucsko, G., P. C. Maurer, N. Y. Yao, M. Kubo, H. J. Noh, P. K. Lo, H. Park, and M. D. Lukin, "Nanometre-scale thermometry in a living cell," *Nature*, Vol. 500, No. 7460, 54–58, Aug. 2013.

[76] Kiyonaka, S., T. Kajimoto, R. Sakaguchi, D. Shinmi, M. Omatsu-Kanbe, H. Matsuura, H. Imamura, T. Yoshizaki, I. Hamachi, T. Morii, and Y. Mori, "Genetically encoded fluorescent thermosensors visualize subcellular thermoregulation in living cells," *Nature Methods*, Vol. 10, No. 12, 1232–1238, Dec. 2013.

[77] Hattori, K., I. Naguro, K. Okabe, T. Funatsu, S. Furutani, K. Takeda, and H. Ichijo, "ASK1 signalling regulates brown and beige adipocyte function," *Nature Communications*, Vol. 7, 11158, Apr. 2016.

[78] Okabe, K., N. Inada, C. Gota, Y. Harada, T. Funatsu, and S. Uchiyama, "Intracellular temperature mapping with a fluorescent polymeric thermometer and fluorescence lifetime imaging microscopy," *Nature Communications*, Vol. 3, 705, Feb. 2012.

[79] Xu, M., X. Zou, Q. Su, W. Yuan, C. Cao, Q. Wang, X. Zhu, W. Feng, and F. Li, "Ratiometric nanothermometer in vivo based on triplet sensitized upconversion," *Nature Communications*, Vol. 9, 2698, Jul. 2018.

[80] Zhu, X., W. Feng, J. Chang, Y.-W. Tan, J. Li, M. Chen, Y. Sun, and F. Li, "Temperature-feedback upconversion nanocomposite for accurate photothermal therapy at facile temperature," *Nature Communications*, Vol. 7, 10437, Feb. 2016.

[81] Zhu, X., J. Li, X. Qiu, Y. Liu, W. Feng, and F. Li, "Upconversion nanocomposite for programming combination cancer therapy by precise control of microscopic temperature," *Nature Communications*, Vol. 9, 2176, Jun. 2018.

[82] Xu, Z., Y. Jiang, J. Ji, E. Forsberg, Y. Li, and S. He, "Classification, identification, and growth stage estimation of microalgae based on transmission hyperspectral microscopic imaging and machine learning," *Optics Express*, Vol. 28, No. 21, 30 686–30 700, 2020.

[83] Gong, D., T. Ma, J. Evans, and S. He, "Deep neural networks for image super-resolution in optical microscopy by using modified hybrid task cascade U-net," *Progress in Electromagnetics Research-pier*, Vol. 171, 185–199, 2021.

[84] Lei, R., X. Liu, F. Huang, D. Deng, S. Zhao, H. Xu, and S. Xu, "Optical thermometry based on anomalous temperature-dependent 1.53 μm infrared luminescence of er in $BaMoO_4$: Er^{3+}/Yb^{3+} phosphor," *Optical Materials*, Vol. 86, 278–285, Dec. 2018.

[85] Li, L., X. Tang, Z. Wu, Y. Zheng, S. Jiang, X. Tang, G. Xiang, and X. Zhou, "Simultaneously tuning emission color and realizing optical thermometry via efficient Tb^{3+}→Eu^{3+} energy transfer in whitlockite-type phosphate multifunctional phosphors," *Journal of Alloys and Compounds*, Vol. 780, 266–275, Apr. 2019.

[86] Yao, Q., P. Hu, P. Sun, M. Liu, R. Dong, K. Chao, Y. Liu, J. Jiang, and H. Jiang, "YAG: Ce^{3+} transparent ceramic phosphors brighten the next-generation laser-driven lighting," *Advanced Materials*, Vol. 32, No. 19, May 2020.

[87] Yu, Z. and X. Sun, "Acousto-optic modulation of photonic bound state in the continuum," *Light Science & Applications*, Vol. 9, No. 1, Jan. 2020.

[88] Shao, Q., G. Zhang, L. Ouyang, Y. Hu, Y. Dong, and J. Jiang, "Emission color tuning of core/shell upconversion nanoparticles through modulation of laser power or temperature," *Nanoscale*, Vol. 9, No. 33, 12 132–12 141, Sep. 2017.

[89] Rodriguez-Sevilla, P., T. Lee, L. Liang, P. Haro-Gonzalez, G. Lifante, X. Liu, and D. Jaque, "Light-activated upconverting spinners," *Advanced Optical Materials*, Vol. 6, No. 12, Jun. 2018.

[90] Wang, N. and S. He, "A simple graphic method for analyzing the polarization state of an optical system with a fixed polarizer and a rotating elliptical retarder," *Progress In Electromagnetics Research*, Vol. 174, 107–114, 2022.

[91] Wu, Y.-D., "High efficiency multi-functional all-optical logic gates based on MIM plasmonic waveguide structure with the Kerr-type nonlinear nano-ring resonators," *Progress In Electromagnetics Research*, Vol. 170, 79–95, 2021.

[92] Kang, Z., C. Mei, L. Zhang, Z. Zhang, J. Evans, Y. Cheng, K. Zhu, X. Zhang, D. Huang, and Y. Li, "Advanced progress on $X^{(3)}$ nonlinearity in chip-scale photonic platforms," *Progress In Electromagnetics Research*, Vol. 170, 17–62, 2021.

[93] Pickel, A. D., A. Teitelboim, E. M. Chan, N. J. Borys, P. J. Schuck, and C. Dames, "Apparent self-heating of individual upconverting nanoparticle thermometers," *Nature Communications*, Vol. 9, Nov. 2018.

[94] Yao, D. Y., P. H. He, H. C. Zhang, J. W. Zhu, M. Hu, and T. J. Cui, "Miniaturized photonic and microwave integrated circuits based on surface plasmon polaritons," *Progress In Electromagnetics Research*, Vol. 175, 105–125, 2022.

[95] Wei, M., H. Ma, C. Sun, C. Zhong, Y. Ye, P. Zhang, R. Liu, J. Li, L. Li, B. Tang, and H. Lin, "TDFA-band silicon optical variable attenuator," *Progress In Electromagnetics Research*, Vol. 174, 33–42, 2022.

[96] Zhu, H., S. Hu, X. Miao, Y. Xiao, and G. Xu, "Electroacupuncture attenuates visceral pain and reverses upregulation of TRPV1 expression in adult rats with neonatal maternal deprivation," *Chinese Medicine*, Vol. 7, No. 1, 1–9, 2016.

[97] Ponnapalli, V. L. N. P., S. Karthikeyan, and J. L. Narayana, "A circular slotted shaped UWB monopole antenna for breast cancer detection," *Progress In Electromagnetics Research*, Vol. 104, 57–65, 2022.

[98] Xing, Y., G. Wang, T. Zhang, F. Shen, L. Meng, L. Wang, F. Li, Y. Zhu, Y. Zheng, N. He, and S. He, "VOC detections with optical spectroscopy," *Progress In Electromagnetics Research*, Vol. 173, 71–92, 2022.

[99] Wang, X.-D., O. S. Wolfbeis, and R. J. Meier, "Luminescent probes and sensors for temperature," *Chemical Society Reviews*, Vol. 42, No. 19, 7834–7869, 2013.

[100] Sedlmeier, A., D. E. Achatz, L. H. Fischer, H. H. Gorris, and O. S. Wolfbeis, "Photon upconverting nanoparticles for luminescent sensing of temperature," *Nanoscale*, Vol. 4, No. 22, 7090–7096, 2012.

[101] Vetrone, F., R. Naccache, A. Zamarron, A. J. d. l. Fuente, F. Sanz-Rodriguez, L. M. Maestro, E. M. Rodriguez, D. Jaque, J. G. Sole, and J. A. Capobianco, "Temperature sensing using fluorescent nanothermometers," *ACS Nano*, Vol. 4, No. 6, 3254–3258, Jun. 2010.

[102] Zimmers, A., L. Aigouy, M. Mortier, A. Sharoni, S. Wang, K. G. West, J. G. Ramirez, and I. K. Schuller, "Role of thermal heating on the voltage induced insulator-metal transition in VO^2," *Physical Review Letters*, Vol. 110, No. 5, Jan. 2013.

[103] Rodriguez-Sevilla, P., Y. Zhang, P. Haro-Gonzalez, F. Sanz-Rodriguez, F. Jaque, J. G. Sole, X. Liu, and D. Jaque, "Thermal scanning at the cellular level by an optically trapped upconverting fluorescent particle," *Advanced Materials*, Vol. 28, No. 12, 2421–2426, Mar. 2016.

[104] Kilbane, J. D., E. M. Chan, C. Monachon, N. J. Borys, E. S. Levy, A. D. Pickel, J. J. Urban, P. J. Schuck, and C. Dames, "Far-field optical nanothermometry using individual sub-50 nm upconverting nanoparticles," *Nanoscale*, Vol. 8, No. 22, 11 611–11 616, 2016.

[105] Janjua, R. A., C. Gao, R. Dai, Z. Sui *et al.*, "Na_+-driven nucleation of $NaYF_4$:Yb,Er nanocrystals and effect of temperature on their structural transformations and luminescent properties," *Journal of Physical Chemistry*, Vol. 122, No. 40, 23242–23250, 2018.

[106] Wang, F., Y. Han, C. S. Lim, Y. Lu, J. Wang, J. Xu, H. Chen, C. Zhang, M. Hong, and X. Liu, "Simultaneous phase and size control of upconversion nanocrystals through lanthanide doping," *Nature*, Vol. 463, No. 7284, 1061–1065, Feb. 2010.

[107] Mai, H.-X., Y.-W. Zhang, L.-D. Sun, and C.-H. Yan, "Size- and phase-controlled synthesis of monodisperse $NaYF_4$:Yb, Er nanocrystals from a unique delayed nucleation pathway monitored with upconversion spectroscopy," *The Journal of Physical Chemistry C*, Vol. 111, No. 37, 13 730–13 739, 2007.

[108] Boyer, J.-C., F. Vetrone, L. A. Cuccia, and J. A. Capobianco, "Synthesis of colloidal upconverting $NaYbF_4$ nanocrystals doped with Er^{3+}, Yb^{3+} and Tm^{3+}, Yb^{3+} via thermal decomposition of lanthanide trifluoroacetate precursors," *Journal of The American Chemical Society*, Vol. 128, No. 23, 7444–7445, 2006.

[109] Chen, B., W. Kong, N. Wang, G. Zhu, and F. Wang, "Oleylamine-mediated synthesis of small $NaYbF_4$ nanoparticles with tunable size," *Chemistry of Materials*, Vol. 31, No. 13, 4779–4786, 2019.

[110] Shan, J. and Y. Ju, "A single-step synthesis and the kinetic mechanism for monodisperse and hexagonal-phase $NaYF_4$:Yb, Er upconversion nanophosphors," *Nanotechnology*, Vol. 20, No. 27, 275603, 2009.

[111] Yi, G., H. Lu, S. Zhao, Y. Ge, W. Yang, D. Chen, and L.-H. Guo, "Synthesis, characterization, and biological application of size-controlled nanocrystalline $NaYF_4$:Yb,Er infrared-to-visible up-conversion phosphors," *Nano Letters*, Vol. 4, No. 11, 2191–2196, 2004.

[112] Yang, Z., P. Gredin, and M. Mortier, "Extremely straightforward room temperature co-precipitation method to synthesize cubic KYF4:Yb/Er up-conversion nanoparticles in deionized water-ethanol solution," *Optical Materials*, Vol. 98, 109458, 2019.

[113] Lin, M., Y. Zhao, S. Q. Wang, M. Liu, Z. F. Duan, Y. M. Chen, F. Li, F. Xu, and T. J. Lu, "Recent advances in synthesis and surface modification of lanthanide-doped upconversion nanoparticles for biomedical applications," *Biotechnology Advances*, Vol. 30, No. 6, 1551–1561, Nov. 2012.

[114] Halimi, I., E. M. Rodrigues, S. L. Maurizio, H.-Q. T. Sun, M. Grewal, E. M. Boase, N. Liu, R. Marin, and E. Hemmer, "Pick your precursor! Tailoring the size and crystal phase of microwave-synthesized sub-10 nm upconverting nanoparticles," *Journal of Materials Chemistry C*, Vol. 7, No. 48, 15 364–15 374, Dec. 2019.

[115] Wang, H.-Q., R. D. Tilley, and T. Nann, "Size and shape evolution of upconverting nanoparticles using microwave assisted synthesis," *Crystengcomm*, Vol. 12, No. 7, 1993–1996, 2010.

[116] Wang, H.-Q. and T. Nann, "Monodisperse upconverting nanocrystals by microwave-assisted synthesis," *ACS Nano*, Vol. 3, No. 11, 3804–3808, Nov. 2009.

[117] Wilhelm, S., M. Kaiser, C. Würth *et al.*, "Water dispersible upconverting nanoparticles: Effects of surface modification on their luminescence and colloidal stability," *Nanoscale*, Vol. 7, No. 4, 1403–1410, Jan. 2015.

[118] Liu, D., X. Xu, Y. Du, X. Qin, Y. Zhang, C. Ma, S. Wen, W. Ren, E. M. Goldys, J. A. Piper, S. Dou, X. Liu, and D. Jin, "Three-dimensional controlled growth of monodisperse sub-50 nm heterogeneous nanocrystals," *Nature Communications*, Vol. 7, 10254, Jan. 2016.

[119] Menyuk, N., K. Dwight, and J. W. Pierce, "$NaYF_4$:Yb, Er — An efficient upconversion phosphor," *Applied Physics Letters*, Vol. 21, No. 4, 159–161, Aug. 1972.

[120] Krämer, K. W., D. Biner, G. Frei, H. U. Güdel, M. P. Hehlen, and S. R. Lüthi, "Hexagonal sodium yttrium fluoride based green and blue emitting upconversion phosphors," *Chemistry of Materials*, Vol. 16, No. 7, 1244–1251, Apr. 2004.

[121] Zheng, K., L. Wang, D. Zhang, D. Zhao, and W. Qin, "Power switched multiphoton upconversion emissions of Er^{3+} in Yb^{3+}/Er^{3+} codoped β-$NaYF_4$ microcrystals induced by 980 nm excitation," *Optics Express*, Vol. 18, No. 3, 2934–2939, 2010.

[122] Som, S., C.-H. Lu, C.-Y. Yang, and S. Das, "Synthesis and design of $NaYF_4$ microprisms via a microwave-assisted approach for highly sensitive optical thermometry applications," *Journal of The American Ceramic Society*, Vol. 104, No. 10, 5168–5181, 2021.

[123] Zhang, Y.-W., X. Sun, R. Si, L.-P. You, and C.-H. Yan, "Single-crystalline and monodisperse LaF_3 triangular nanoplates from a single-source precursor," *Journal of the American Chemical Society*, Vol. 127, No. 10, 3260–3261, 2005.

[124] Shan, J., X. Qin, N. Yao, and Y. Ju, "Synthesis of monodisperse hexagonal $NaYF_4$:Yb, Ln (Ln=Er, Ho and Tm) upconversion nanocrystals in TOPO," *Nanotechnology*, Vol. 18, No. 44, 445607, 2007.

[125] Shan, J. and Y. Ju, "Controlled synthesis of lanthanide-doped $NaYF_4$ upconversion nanocrystals via ligand induced crystal phase transition and silica coating," *Applied Physics Letters*, Vol. 91, No. 12, Sep. 2007.

[126] Yi, G.-S. and G.-M. Chow, "Water-soluble $NaYF_4$:Yb, Er(Tm)/$NaYF_4$/polymer core/shell/shell nanoparticles with significant enhancement of upconversion fluorescence," *Chemistry of Materials*, Vol. 19, No. 3, 341–343, 2007.

[127] Mai, H.-X., Y.-W. Zhang, R. Si, Z.-G. Yan, L.-D. Sun, L.-P. You, and C.-H. Yan, "High-quality sodium rare-earth fluoride nanocrystals: controlled synthesis and optical properties," *Journal of the American Chemical Society*, Vol. 128, No. 19, 6426–6436, May 2006.

[128] Boyer, J.-C., L. A. Cuccia, and J. A. Capobianco, "Synthesis of colloidal upconverting $NaYF_4:Er^{3+}/Yb^{3+}$ and Tm^{3+}/Yb^{3+} monodisperse nanocrystals," *Nano Letters*, Vol. 7, No. 3, 847–852, 2007.

[129] Yi, G. S. and G. M. Chow, "Synthesis of hexagonal-phase $NaYF_4$:Yb, Er and $NaYF_4$:Yb, Tm nanocrystals with efficient up-conversion fluorescence," *Advanced Functional Materials*, Vol. 16, No. 18, 2324–2329, 2006.

[130] Mai, H.-X., Y.-W. Zhang, L.-D. Sun, and C.-H. Yan, "Size- and phase-controlled synthesis of monodisperse $NaYF_4$:Yb,Er nanocrystals from a unique delayed nucleation pathway monitored with upconversion spectroscopy," *Journal of Physical Chemistry C*, Vol. 111, No. 37, 13 730–13 739, Sep. 2007.

[131] Boyer, J.-C., F. Vetrone, L. A. Cuccia, and J. A. Capobianco, "Synthesis of colloidal upconverting nayf nanocrystals doped with Er^{3+}, Yb^{3+} and Tm^{3+}, Yb^{3+} via thermal decomposition of lanthanide trifluoroacetate precursors," *Journal of The American Chemical Society*, Vol. 128, No. 23, 7444–7445, Jun. 2006.

[132] Liu, C., H. Wang, X. Li, and D. Chen, "Monodisperse, size-tunable and highly efficient β-$NaYF_4$:Yb, Er (Tm) upconversion luminescent nanospheres: controllable synthesis and their surface modifications," *Journal of Materials Chemistry*, Vol. 19, No. 21, 3546–3553, 2009.

[133] Li, Z. and Y. Zhang, "Monodisperse silica-coated polyvinylpyrrolidone/$NaYF_4$ nanocrystals with multicolor upconversion fluorescence emission," *Angewandte Chemie*, Vol. 118, No. 46, 7896–7899, 2006.

[134] Li, Z. and Y. Zhang, "An efficient and user-friendly method for the synthesis of hexagonal-phase $NaYF_4$:Yb, Er/Tm nanocrystals with controllable shape and upconversion fluorescence," *Nanotechnology*, Vol. 19, No. 34, 345606, 2008.

[135] Ehlert, O., R. Thomann, M. Darbandi, and T. Nann, "A four-color colloidal multiplexing nanoparticle system," *ACS Nano*, Vol. 2, No. 1, 120–124, Jan. 2008.

[136] Wang, F. and X. Liu, "Upconversion multicolor fine-tuning: visible to near-infrared emission from lanthanide-doped $NaYF_4$ nanoparticles," *Journal of the American Chemical Society*, Vol. 130, No. 17, 5642–5643, 2008.

[137] Janjua, R. A., O. Iqbal, M. A. Ahmed, A. A. Al-Kahtani, S. Saeed, M. Imran, and A. G. Wattoo, "Homo-hetero/core-shell structure design strategy of $NaYF_4$ nanocrystals for superior upconversion luminescence," *RSC Advances*, Vol. 11, No. 34, 20 746–20 751, 2021.

[138] Haase, M. and H. Schaefer, "Upconverting nanoparticles," *Angewandte Chemie-International Edition*, Vol. 50, No. 26, 5808–5829, 2011.

[139] Whitesides, G. M., "The 'right' size in nanobiotechnology," *Nature Biotechnology*, Vol. 21, No. 10, 1161–1165, Oct. 2003.

[140] Ostrowski, A. D., E. M. Chan, D. J. Gargas, E. M. Katz, G. Han, P. J. Schuck, D. J. Milliron, and B. E. Cohen, "Controlled synthesis and single-particle imaging of bright, sub-10 nm lanthanide-doped upconverting nanocrystals," *ACS Nano*, Vol. 6, No. 3, 2686–2692, Mar. 2012.

[141] Heer, S., K. Kömpe, H.-U. Güdel, and M. Haase, "Highly efficient multicolour upconversion emission in transparent colloids of lanthanide-doped $NaYF_4$ nanocrystals," *Advanced Materials*, Vol. 16, No. 23-24, 2102–2105, Dec. 2004.

[142] Heer, S., O. Lehmann, M. Haase, and H. Güdel, "Blaue, grüne und rote upconversion-emission von lanthanoid-dotierten $LuPO_4$-und $YbPO_4$-nanokristallen in transparenter kolloidaler lösung," *Angewandte Chemie*, Vol. 115, No. 27, 3288–3291, Jul. 2003.

[143] Schäfer, H., P. Ptacek, H. Eickmeier, and M. Haase, "Synthesis of hexagonal Yb^{3+}, Er^{3+}-doped $NaYF_4$ nanocrystals at low temperature," *Adv Funct Mater*, Vol. 19, No. 19, 3091–3097, Oct. 2009.

[144] Ostrowski, A. D., E. M. Chan, D. J. Gargas, E. M. Katz, G. Han, P. J. Schuck, D. J. Milliron, and B. E. Cohen, "Controlled synthesis and single-particle imaging of bright, sub-10 nm lanthanide-doped upconverting nanocrystals," *ACS Nano*, Vol. 6, No. 3, 2686–2692, Mar. 2012.

[145] Rinkel, T., A. N. Raj, S. Dühnen, and M. Haase, "Synthesis of 10 nm β-$NaYF_4$:Yb,Er/$NaYF_4$ core/shell upconversion nanocrystals with 5 nm particle cores," *Angewandte Chemie International Edition*, Vol. 55, No. 3, 1164–1167, Jan. 2016.

[146] Rinkel, T., J. Nordmann, A. N. Raj, and M. Haase, "Ostwald-ripening and particle size focussing of sub-10 nm $NaYF_4$ upconversion nanocrystals," *Nanoscale*, Vol. 6, No. 23, 14 523–14 530, 2014.

[147] Wang, G., W. Qin, L. Wang, G. Wei, P. Zhu, and R. Kim, "Intense ultraviolet upconversion luminescence from hexagonal $NaYF_4:Yb^{3+}/Tm^{3+}$ microcrystals," *Optics Express*, Vol. 16, No. 16, 11 907–11 914, 2008.

[148] Jahanbazi, F. and Y. Mao, "Recent advances on metal oxide-based luminescence thermometry," *Journal of Materials Chemistry C*, Vol. 9, No. 46, 16 410–16 439, Dec. 2021.

[149] McLaurin, E. J., L. R. Bradshaw, and D. R. Gamelin, "Dual-emitting nanoscale temperature sensors," *Chemistry of Materials*, Vol. 25, No. 8, 1283–1292, Apr. 2013.

[150] Cheng, Y., Y. Gao, H. Lin, F. Huang, and Y. Wang, "Strategy design for ratiometric luminescence thermometry: circumventing the limitation of thermally coupled levels," *Journal of Materials Chemistry C*, Vol. 6, No. 28, 7462–7478, Jul. 2018.

[151] Wade, S. A., S. F. Collins, and G. W. Baxter, "Fluorescence intensity ratio technique for optical fiber point temperature sensing," *Journal of Applied Physics*, Vol. 94, No. 8, 4743–4756, 2003.

[152] Wawrzynczyk, D., A. Bednarkiewicz, M. Nyk, W. Strek, and M. Samoc, "Neodymium(iii) doped fluoride nanoparticles as non-contact optical temperature sensors," *Nanoscale*, Vol. 4, No. 22, 6959–6961, 2012.

[153] Geitenbeek, R. G., P. T. Prins, W. Albrecht, A. van Blaaderen, B. M. Weckhuysen, and A. Meijerink, "$NaYF_4$:Er^{3+},Yb^{3+}/SiO_2 core/shell upconverting nanocrystals for luminescence thermometry up to 900 K," *The Journal of Physical Chemistry C*, Vol. 121, No. 6, 3503–3510, 2017.

[154] Li, L., F. Qin, Y. Zhou, Y. Zheng, H. Zhao, and Z. Zhang, "Exploiting the Yb^{3+} and Er^{3+} codoped β-$NaYF_4$ nanoparticles as luminescent thermometers for white-led-free thermal sensing at the nanoscale," *ACS Applied Nano Materials*, Vol. 1, No. 4, 1912–1920, 2018.

[155] Runowski, M., N. Stopikowska, D. Szeremeta, S. Goderski, M. Skwierczyńska, and S. Lis, "Upconverting lanthanide fluoride core@ shell nanorods for luminescent thermometry in the first and second biological windows: β-$NaYF_4$:Yb^{3+}-Er^{3+}@ SiO_2 temperature sensor," *ACS Appl Mater Interfaces*, Vol. 11, No. 14, 13 389–13 396, Apr. 2019.

[156] Mi, C., J. Zhou, F. Wang, G. Lin, and D. Jin, "Ultrasensitive ratiometric nanothermometer with large dynamic range and photostability," *Chemistry of Materials*, Vol. 31, No. 22, 9480–9487, Nov. 2019.

[157] Wang, Y., L. Lei, R. Ye, G. Jia, Y. Hua, D. Deng, and S. Xu, "Integrating positive and negative thermal quenching effect for ultrasensitive ratiometric temperature sensing and anticounterfeiting," *ACS Applied Materials & Interfaces*, Vol. 13, No. 20, 23 951–23 959, May 2021.

[158] Wu, X., S. Zhan, J. Han, and Y. Liu, "Nanoscale ultrasensitive temperature sensing based on upconversion nanoparticles with lattice self-adaptation," *Nano Letters*, Vol. 21, No. 1, 272–278, Jan. 2021.

[159] Trejgis, K., K. Ledwa, A. Bednarkiewicz, and L. Marciniak, "A single-band ratiometric luminescent thermometer based on tetrafluorides operating entirely in the infrared region," *Nanoscale Advances*, Vol. 4, No. 2, 437–446, Jan. 2022.

[160] Marciniak, L., A. Pilch, S. Arabasz, D. Jin, and A. Bednarkiewicz, "Heterogeneously Nd^{3+} doped single nanoparticles for NIR-induced heat conversion, luminescence, and thermometry," *Nanoscale*, Vol. 9, No. 24, 8288–8297, 2017.

[161] Cai, Z., S. Kang, X. Huang, X. Song, X. Xiao, J. Qiu, and G. Dong, "A novel wide temperature range and multi-mode optical thermometer based on bi-functional nanocrystal-doped glass ceramics," *Journal of Materials Chemistry C*, Vol. 6, No. 37, 9932–9940, Oct. 2018.

[162] Pilch-Wróbel, A., K. Ledwa, A. Kotulska, and A. Bednarkiewicz, "The influence of Ce^{3+} codoping on upconversion in nanocrystalline $NaYF_4$:Yb^{3+}, Tm^{3+}," *Journal of Luminescence*, Vol. 251, 119116, Nov. 2022.

[163] Yao, H., H. Shen, and Q. Tang, "Enhanced upconversion luminescence and temperature sensitivity of $NaYF_4$:Er,Yb phosphors via Mn doping," *Materials Research Express*, Vol. 6, No. 12, 125017, Nov. 2019.

[164] Ryszczyńska, S., I. R. Martín, and T. Grzyb, "Near-infrared optical nanothermometry via upconversion of Ho_{3+}-sensitized nanoparticles," *Sci. Rep.*, Vol. 13, No. 1, 14819, Sep. 2023.

[165] Cao, B., Y. Bao, Y. Liu, J. Shang, Z. Zhang, Y. He, Z. Feng, and B. Dong, "Wide-range and highly-sensitive optical thermometers based on the temperature-dependent energy transfer from Er to Nd in Er/Yb/Nd codoped $NaYF_4$ upconversion nanocrystals," *Chemical Engineering Journal*, Vol. 385, 123906, Apr. 2020.

[166] Chen, X., J. Sun, H. Zhao, K. Yang, Y. Zhu, H. Luo, K. Yu, H. Fan, and X. Zhang, "Theranostic system based on $NaY(Mn)F_4$:Yb/er upconversion nanoparticles with multi-drug resistance reversing ability," *Journal of Materials Chemistry B*, Vol. 6, No. 21, 3586–3599, 2018.

[167] Ba, Z., M. Hu, Y. Zhao, Y. Wang, J. Wang, and Z. Zhang, "Double nir laser stimulation and enhancing the thermal sensitivity of Er^{3+}/Tm^{3+}/Nd^{3+} doped multilayer core-shell nanoparticles," *Nanotechnology*, Vol. 29, No. 35, 355704, 2018.

[168] Janjua, R. A., U. Farooq, R. Dai, Z. Wang, and Z. Zhang, "Wide-range ratiometric upconversion luminescence thermometry based on non-thermally coupled levels of Er in high-temperature cubic phase $NaYF_4$:Yb,Er," *Optics Letters*, Vol. 44, No. 19, 4678–4681, 2019.

[169] Nie, J., W. Ying, X. Fan, S. Xu, Z. Gao, J. Gu, and S. Liu, "Cryogenic dependent energy manipulation in nonthermally coupled levels for multicolor upconversion luminescence," *Journal of Physical Chemistry C*, Vol. 125, No. 34, 19 040–19 047, Sep. 2021.

[170] Cheng, Z., M. Meng, J. Wang, Z. Li, J. He, H. Liang, X. Qiao, Y. Liu, and J. Ou, "High-sensitivity $NaYF_4$:Yb^{3+}/Ho^{3+}/Tm^{3+} phosphors for optical temperature sensing based on thermally coupled and non-thermally coupled energy levels," *Nanoscale*, Vol. 15, No. 26, 11 179–11 189, 2023.

[171] Martins, J. C., A. R. N. Bastos, R. A. S. Ferreira, X. Wang, G. Chen, and L. D. Carlos, "Primary luminescent nanothermometers for temperature measurements reliability assessment," *Advanced Photonics Research*, Vol. 2, No. 5, May 2021.

[172] Meng, M., T. Zhang, J. Wang, Z. Cheng, J. Yang, X. Qiao, J. Wen, U. Resch-Genger, and J. Ou, "Fluorescence temperature sensing of $NaYF_4$:Yb^{3+}/Tm^{3+}@ $NaGdF_4$:Nd^{3+}/Yb^{3+} nanoparticles at low and high temperatures," *Nanotechnology*, Vol. 33, No. 45, 455502, 2022.

[173] Xu, W., L. Zhao, F. Shang, L. Zheng, and Z. Zhang, "Modulating the thermally coupled status of energy levels in rare earth ions for sensitive optical temperature sensing," *Journal of Luminescence*, Vol. 249, 119042, Sep. 2022.

[174] Marciniak, L., K. Prorok, L. Francés-Soriano, J. Pérez-Prieto, and A. Bednarkiewicz, "A broadening temperature sensitivity range with a core-shell YbEr@YbNd double ratiometric optical nanothermometer," *Nanoscale*, Vol. 8, No. 9, 5037–5042, 2016.

[175] Li, H., F. Wei, Y. Li, M. Yu, Y. Zhang, L. Liu, and Z. Liu, "Optical fiber sensor based on upconversion nanoparticles for internal temperature monitoring of Li-ion batteries," *Journal of Materials Chemistry C*, Vol. 9, No. 41, 14 757–14 765, Oct. 2021.

[176] Ning, X., N. Liu, J. Liu, Y. Wu, J. Qian, W. Zhang, and W. Gu, "Temperature sensing and bioimaging realized in $NaErF_4$:40%Tm@$NaYF_4$ with extremely intense red upconversion and suitable R/G emission ratio," *Optical Materials*, Vol. 131, 112659, Sep. 2022.